

1 This manuscript is a preprint

2 This manuscript will be submitted to Basin Research

3 Subsequent versions of this manuscript may have different content. If accepted, the final version of this manuscript  
4 will be available via the 'Peer reviewed Publication DOI' link through this webpage. Please feel free to contact  
5 us privately at [ovie.eruteya@unige.ch](mailto:ovie.eruteya@unige.ch) or [@SeisImaged\\_Ovie](https://twitter.com/SeisImaged_Ovie). We eagerly await your comments and feedback on  
6 this manuscript. Thank you for your time and effort.

7

1 **Evolution of seafloor pockmarks along the Northern Orange Basin, Offshore South Africa: Interplay**  
2 **between fluid flow and bottom current activities**

3 Ovie Emmanuel Eruteya<sup>1\*</sup>; Nehemiah Dominick<sup>2</sup>, Yakufu Niyazi<sup>3</sup>, Emna Meftah <sup>1</sup>, Kamaldeen O. Omosanya<sup>4,5</sup>  
4 and Mimonitu Opuwari<sup>2</sup>, Andrea Moscariello<sup>1</sup>

5

6 <sup>1</sup>Geo-Energy, Reservoir Geology and Basin Analysis Group, Department of Earth Sciences, University of Geneva,  
7 Geneva, Switzerland.

8 <sup>2</sup>Department of Geology, University of Western Cape, Cape Town, South Africa.

9 <sup>3</sup>School of Life and Environmental Sciences, Deakin University, Warrnambool, Australia.

10 <sup>4</sup>Oasisgeokonsult, Trondheim. 7052, Norway

11 <sup>5</sup>Department of Geoscience, University of Malta. Msida, Malta

12

13 \*Corresponding Author: Ovie Emmanuel Eruteya

14 Email: Ovie.Eruteya@unige.ch

15

16

17

18

19

20

21

22

23

24

25

26

27

28

29

30

31

32

33

34

35

36

37

38

39

40

1 **Acknowledgements**

2 OEE acknowledges the receipt of the Swiss Government Postdoctoral Scholarship for Excellence Furthermore.  
3 Schlumberger is acknowledged for granting the academic license of Petrel to the University of Geneva, the  
4 University of Western Cape, and Deakin University. ESRI is also acknowledged for granting the academic license  
5 of ArcGIS to the University of Geneva and Deakin University. Finally, Shell and the Petroleum Agency of South  
6 Africa (PASA) are acknowledged for donating the 3-D seismic reflection survey analysed in this study to The  
7 University of Western Cape.

8  
9  
10  
11  
12  
13  
14  
15  
16  
17  
18  
19  
20  
21  
22  
23  
24  
25  
26  
27  
28  
29  
30  
31  
32  
33  
34  
35  
36  
37  
38  
39  
40

1 **Abstract**

2 Pockmarks are pervasive geomorphologic features identified along continental margins resulting from fluid  
3 expulsion on the seafloor. However, the understanding of the underlying geological mechanism/control in relation  
4 to their evolution, distribution, and morphology is limited, especially along data-starved continental margins such  
5 as the Northern Orange Basin. Analysis of a high-quality 3D seismic reflection data reveals at least 50 individual  
6 pockmarks, two channel-like depressions and several irregular depressions in water depth ranging between 800  
7 m and 2400 m. Morphologically, the pockmarks are circular, elongated, comet-like and crescentic in shape, with  
8 diameters and depths ranging between ~0.2 - 2.8 km and ~10 - 130 m, respectively. Preferential alignment of  
9 these pockmarks on the seafloor in relation to the axis of underlying turbidite channels, erosional morphologies  
10 and mass transport complexes portray a genetic relationship. The slope architecture hints at the possibility of both  
11 deep and shallow fluid source driving pockmark formation. Under this scenario, deep thermogenic gas derived  
12 from Cretaceous source rocks migrated along fault systems associated with the Late Cretaceous Megalide  
13 complex to the overburden. The fluids are stored/redistributed in contourite and turbidite channels and  
14 subsequently focused toward the seafloor under an increased pore pressure regime. Yet, the fluids may be either  
15 solely biogenic gas or heterogeneous, incorporating biogenic components and pore-water derived from the  
16 channels and dewatering of the contourites. Importantly, the discovery of crescentic and elongated end-member  
17 pockmark morphologies indicate post-formation sculpting of the initial pockmark morphologies by bottom  
18 currents. The discovery of these deep-water pockmarks opens the possibility that such fluid escape features may  
19 be more widespread than currently documented in the Northern Orange Basin. This has implications in  
20 understanding of the petroleum system here and their potential role in the South Atlantic marine ecosystems and  
21 global climate change in terms of the expulsion of climate forcing gases.

22

23 **Keywords:** Pockmarks, Turbidite channels, Mass Transport Deposits Contourites, Orange Basin, Offshore South  
24 Africa, South Atlantic margin.

25

26

27

28

29

30

31

32

33

34

35

36

37

38

## 1 **1.0 Introduction**

2 Fluid escape features such as pockmarks are common features observed on seafloors along many continental  
3 margins (Berndt, 2005; Cartwright et al., 2007; Gay et al., 2007; Andresen, 2012; Anka, Berndt and Gay, 2012,  
4 Omeru et al., 2021, Kumar et al., 2021). Pockmarks are sub-circular to semi-elongated crater-like depressions  
5 evolving from focused fluid flow and expulsion of gases along the seafloor (Judd and Hovland, 2007; Pilcher and  
6 Argent, 2007; Sun et al., 2011). However, seafloor processes, such as bottom currents, postdating the original  
7 pockmark formation, can modify their initial sub-circular morphology, and create new end-member series such  
8 as crescentic, comet-like, and elongated pockmarks (Schattner et al., 2016; Sun et al., 2011). The evolution of  
9 pockmarks in marine sediments has important implications on sustaining marine ecosystems as escaping methane  
10 serves as a source of food for fostering the development of chemosynthetic habitats, global warming via expulsion  
11 of climate-forcing gases and, slope stability (Berndt, 2005; Judd and Hovland, 2007). From an economic  
12 perspective, the presence of pockmarks may likewise be proxies for leakage from deep prospective hydrocarbon  
13 reservoirs (Heggland, 1998, Anka et al., 2012).

14  
15 Pockmarks may be isolated, clustered, or aligned, revealing subsurface structural or stratigraphic control on fluid  
16 flow and escape. Spatial distribution of pockmarks on the seafloor may be related to underlying fault systems,  
17 (faulted) anticlines, mud/salt diapirs, gas hydrates and submarine mass transport complex, paleochannels and  
18 canyons (Gay et al., 2007; Pilcher and Argent, 2007; Riboulot et al., 2013; Eruteya et al., 2018; Roelofse et al.,  
19 2020; Kumar et al., 2021). However, the geological processes modulating fluid plumbing and sustaining long term  
20 fluid escape along continental margins remains poorly understood, especially in data-starved deep-water settings  
21 (Eruteya et al., 2018) such as the Northern Orange Basin in the eastern South Atlantic Ocean.

22  
23 The eastern South Atlantic margin has not been the target of intensive seafloor mapping (Wenau et al., 2021),  
24 especially the Orange Basin, offshore South Africa (Palan et al., 2020). This has resulted in a limited  
25 understanding of the abundance, distribution, and geological controls of seafloor fluid escape features. Previous  
26 studies have focused on the southern segment of the Orange Basin, where fluid flow elements encompassing  
27 pockmarks, mud volcanoes, chimneys, and pipes were documented (Viola et al. 2005; Hartwig, Anka, & di Primio  
28 2012; Isiaka et al. 2017; Palan et al. 2020) and only recently several pockmark features have been identified in  
29 the northern segment of the deep-water Orange Basin (Mahlalela et al., 2021). These fluid flow features are linked  
30 to an active hydrocarbon system (Hartwig et al., 2012; Palan et al., 2020). However, as hydrocarbon exploration  
31 transits into deep waters (> 500 m) in the Northern Orange Basin, more subsurface exploration datasets have  
32 become available in recent times, allowing the investigation of subsurface fluid flow dynamics in this area.

33  
34 In this study, analysis of a new high-quality 3D seismic reflection dataset from the slope of the Northern Orange  
35 Basin, reveals at least 50 individual pockmarks and other intricate depressions on the seafloor (Figure 1). We aim  
36 to characterize these pockmarks and unravel their genetic mechanism. Detailed seismic interpretation revealed  
37 that these pockmarks are not randomly developed, and their spatial distribution on the seafloor is controlled by a  
38 buried turbidite channel system and other erosional features. Notably, some of these pockmarks reveal evidence  
39 of post-formation modification arising from the sculpting activities of the South Atlantic bottom currents in the  
40 study area. The findings from this study reveal an intriguing interplay between subsurface fluid flow and

1 oceanographic processes in developing seafloor features documented along this segment of the South Atlantic  
2 Ocean.

## 3 4 **2.0 Geological and oceanographic setting of the Orange Basin**

5 The study area is situated along the continental slope of the South-African segment of the Northern Orange Basin  
6 (Figure 1). The Orange Basin hosts substantial hydrocarbon reserves (Brown et al., 1995; Van der Spuy, 2003;  
7 Paton et al., 2007; Kuhlmann et al., 2010) within the basin fill of up to 3 km in the southern segment and reaching  
8 7 km in the northern segment (Palan et al., 2021). The Orange Basin is a rift-drift basin created from the continental  
9 break-up and subsequent rifting of South America from Africa in the Late Jurassic to Early Cretaceous (Van der  
10 Spuy, 2003). A series of rift-related and approximately SE-NW orientated grabens, and half-grabens (Figure 2a  
11 and b) were formed in the basin during the break-up of Gondwana during the Late Jurassic to Early Cretaceous  
12 (Nürnberg & Müller, 1991; Macdonald et al., 2003). The rift stage was characterized by the deposition of volcanic  
13 successions with siliciclastic and lacustrine sediments (Figure 2) (Gerrard and Smith, 1982; Kuhlmann et al.,  
14 2010). During the transitional stage from the Barremian-Aptian, fluvial beds and overlying marine sands were  
15 deposited (Figure 2) (Brown, 1995; Kuhlmann et al., 2010). The post-rift phase was established during the Late  
16 Aptian and was characterized by thermal subsidence of the margin and the initiation of open ocean circulation  
17 (Figure 2) (Pedley, 1990). At the beginning of this stage, restricted marine, deltaic and coastal plain settings  
18 associated with the sediment input from the north by the Orange River system concentrated in the depocenters  
19 along the present-day shelf area from the Mid to Late Cretaceous (PESA, 2018). Importantly, deposition of the  
20 Aptian succession represents the onset of the drift phase of sedimentation within the Orange Basin (Brown et al.,  
21 1995). This interval also contains black shales that represent potential source rocks in the Orange Basin (Van der  
22 Spuy, 2003). Likewise, the Cenomanian-Turonian Shales deposited in the basin are also important source rocks  
23 (Aldrich et al., 2003).

24 During the Cenozoic, subsidence rate decreased, and the depocenter shifted basinward, forming vertically stacked  
25 aggradational sequences along the slope (Dingle & Scrutton, 1974; PESA, 2018). In parallel, sedimentary  
26 composition transited from Late Cretaceous siliciclastic clays and siltstones with occasional sandy layers to  
27 Cenozoic mixed carbonates, siliciclastics and authigenic sediments (Figure 2) (Gerrard & Smith, 1982; Hartwig  
28 et al., 2012). Gravity-driven deformations and bottom-current related remobilization of sediments have been  
29 recognized as essential processes during the post-rift evolution of the Orange Basin and in the broader margin of  
30 southwestern Africa (Figures 2a and 2b) (de Vera et al., 2010; Scarselli et al., 2016; Dalton et al., 2017). The onset  
31 of a significant phase of slope failure occurred in the Late Cretaceous when a series of short-lived gravitational  
32 collapse episodes occurred along the middle and upper slope of the basin margin from the mid-Aptian to Santonian  
33 (100–80 Ma) (de Vera et al., 2010). The accelerated margin uplift and increased pressure of organic-rich shale  
34 units within the Turonian basal detachments are the main reasons for the formation of the late Cretaceous  
35 Megaslide complex (Figures 2a and b) (de Vera et al., 2010; Scarselli et al., 2016). Structurally, the gravity-driven  
36 failures in the study area are characterized by extensional growth faults, large-scale slumping, toe-thrust faults,  
37 and fault-related folds (Figures, 1b and 3). Numerous repeated shallow collapse failures occur within the  
38 Oligocene to recent successions, which is also incised by a series of stacked contourites (Scarselli et al., 2016).  
39 These contourite deposits are thought to be initiated by establishing the northward Benguela Current (Weigelt &  
40 Uenzelmann-Neben, 2004).

1 The Orange Basin is affected by four main oceanic current systems encompassing the Antarctic Bottom Water  
2 (AABW), the North Atlantic Deep Water (NADW), the Antarctic Intermediate Water (AAIW) and the Benguela  
3 Coastal Currents (BCC) (Weigelt and Uenzelmann-Neben, 2004) (Figure 1). The AABW is the deepest bottom  
4 current operating at a water depth  $> 4000$  m and interacting with the Lower continental slope (Palan et al 2021).  
5 The NADW and AAIW are counter-currents flowing south-easterly and north-westerly respectively (Weigelt &  
6 Uenzelmann-Neben, 2004; Uenzelmann-Neben & Huhn, 2009) (Figure 1). The NADW flows between 1500 –  
7 4000 m water depth compared to shallower AAIW operating in water depth of between 500 and 1500 m. The  
8 BCC overlies the AAIW flowing equatorward from water depth of approximately 500 m (Shannon, 1985).

### 9 10 **3.0 Dataset and Methodology**

11 The 3D seismic reflection dataset used in this study is a 2730 km<sup>2</sup> cropped volume of a pre-stack time-migrated  
12 seismic survey (named as Shell SA OB12) in the Orange Basin, northwest of the Ibhuesi gas field (Figure 1).  
13 This survey was acquired using a 4100 in<sup>3</sup> airgun array placed  $8 \pm 1$  m below the sea level. A 25 m shot interval,  
14 and 8 km long streamer with 636 channels with a group interval of 12.5 m was used. The record length reached  
15 7.2 s two-way time (TWT), with a vertical sampling interval of 2 ms and a fold of 80. The data has a bin spacing  
16 of 25 m  $\times$  25 m for inlines (NW–SE direction) and crosslines (NE–SW direction). The seismic data is zero-phased  
17 at the seabed reflection and displayed with normal SEG (Society of Exploration Geophysicists) polarity such that  
18 a decrease in acoustic impedance with depth at lithologic boundaries are shown as blue reflections or troughs,  
19 while red reflections or peaks are increases in acoustic impedance with depth. Given a dominant frequency of  $\sim 50$   
20 Hz and velocity of 1800 m/s for the near seafloor sediments, the vertical resolution ( $\lambda/4$ ), is estimated at 9 m.  
21 Therefore, seafloor pockmarks and other depressions are within the resolvable limits of the seismic reflection  
22 dataset. The limit of detectability ( $\lambda/32$ ) is estimated at  $\sim 1.13$  m. Vertical structures less than this height will not  
23 be detected in the seismic data.

24  
25 Furthermore, we relied on the seismic stratigraphic framework of previous studies from the Orange Basin in  
26 interpreting key reflections in the seismic data (Sallomo, 2012; Mahlalela et al., 2021). A velocity of 1500 m/s  
27 was used in time to depth conversion of the seafloor surface interpreted from the 3D seismic data (Wefer et al.,  
28 1998). Subsequently, the depth-converted surface was used as an input for the semi-automatic depression mapping  
29 workflow developed by Gaferia et al. (2012) in QGIS. For each pockmark, the depth, area, perimeter, and water  
30 depth were extracted from the bathymetry map (Figure 3). When the pockmark displays non-circular geometry,  
31 the diameter of the pockmark is measured along the long axis. Variance (trace-to-trace variability of seismic data)  
32 attribute horizon probe was extracted at 100 ms TWT below the seafloor using a smoothed version of the seafloor  
33 structural map using the geo-body interpretation probe tool in Petrel 2020. Variance attribute is an edge detection  
34 volume-based geometric attribute that allows regions of surface discontinuities to be illuminated (Ostanin et al.,  
35 2012; Niyazi et al., 2018). It is particularly useful in delineating features such as channels and faults of implication  
36 to fluid flow (Eruteya et al., 2016; Niyazi et al., 2021). On the variance maps, regions having similar traces  
37 (undeformed) exhibit low variance coefficients compared to high variance coefficients for regions characterized  
38 by discontinuities.

## 1 **4.0 Results**

### 2 **4.1 Seismic stratigraphy of the Northern South-African Slope**

3 The seismic characteristic of the slope is shown on the dip section from the Seafloor (Horizon S) down to 5 s  
4 TWT. The study area is subdivided into four main seismic stratigraphic units using regionally recognized  
5 reflections from previous studies in the Orange Basin (de Vera et al., 2010, Sallomo, 2012, Mahlalela et al., 2021)  
6 (Figures 2b and 4).

#### 7 8 **Seismic Unit 1 (SU1) - (Pre) Cenomanian to Turonian**

9 The basal seismic sequence SU1 consists of two separable sub-units SU1a and SU1b (Figure 4). These sub-units  
10 are separated by the Cenomanian/Turonian (93 Ma) unconformity. SU1a is characterized by semi continuous  
11 reflectors with variable amplitude ranging from low to high. On the other hand, SU1b is characterized by chaotic,  
12 low to moderate amplitude reflections that are related to gravity-driven tectonics (Figure 4). SU1a is composed of  
13 Organic rich shales, compared to the Turonian marine shales in SU1b (de Vera et al., 2010, Scarselli, 2016,  
14 Mahlalela, 2021).

#### 15 16 **Seismic Unit 2 (SU2) - Late Cretaceous Megaslides Complex**

17 This unit is bounded by the Turonian detachment level at the base and the top megaslides horizon TM (Figure 4).  
18 In the cross section within the study area, the extensional domain, transitional domain, and compressional domain  
19 at toe of the gravity-driven megaslides complex comprises the SU2. (Figure 4). This unit is composed of variable  
20 seismic facies that encompasses chaotic to moderate-high amplitude, semi-continuous reflections that form  
21 compartmentalized blocks deformed by the thrust fault system in the toe domain and extensional faults in the  
22 extensional domain (Figure 4).

#### 23 24 **Seismic Unit 3 (SU3) - Santonian to Maastrichtian**

25 This unit is bounded by the horizon TM at the base and base Palaeocene (P) horizon at the top. However, the  
26 presence of the prominent Late Maastrichtian unconformity (Horizon M) permits further subdividing this unit into  
27 two subunits: SU3a and SU3b. SU3a consists of moderate-high amplitude semi-continuous reflections (Figure 4).  
28 The sediments within this subunit occupy the accommodation space provided by the underlying Late Cretaceous  
29 Megaslides Complex (Figure 4). SU3b is bounded at the base by the major Late Maastrichtian unconformity  
30 (Horizon M). It is characterized by moderate to high amplitude, continuous reflections (Figure 4). This subunit  
31 is interpreted as a marine condensed section and is likely composed of hemipelagic and pelagic sediments  
32 (Salomo, 2012).

#### 33 34 **Seismic Unit 4 (SU4) Base Paleocene to Recent**

35 SU 4 represents the Cenozoic basin fill and is bounded at the base by Horizon P – the base of the Paleocene and  
36 at the top by Horizon S-seafloor (Figure 4). Some faults deform this interval and detach into the underlying  
37 Cretaceous sediments (Figure 4). This unit is further subdivided into three subunits: SU4a, SU4b and SU4c. The  
38 oldest part of this unit SU4a is characterized by laterally continuous, moderate to high-amplitude reflections  
39 (Figure 4). In comparison, overlying SU4b is composed of buried contourite drifts and buried mass transport  
40 complexes (MTCs) emplaced during episodes of slope instabilities. The MTCs are characterized by semi-

1 transparent and chaotic seismic reflections with mappable base and top surfaces (Frey-Martinez et al., 2005; Bull  
2 et al., 2009; Eruteya et al., 2021). SU4b is assigned an Oligocene-Miocene age, corresponding to the onset of  
3 bottom current activities related to contourite deposition in the Orange Basin (Uenzelmann-Neben et al., 2007).  
4 The youngest subunit SU4c is characterized by laterally continuous and low-moderate amplitude reflections. Also,  
5 MTC is emplaced within this subunit represented by chaotic low amplitude reflections. Importantly, multiple U-  
6 and V-shaped depressions develop within this unit and along the seafloor reflector topping this subunit (Figure  
7 4). Analysis of ODP Leg 175 Hole 1087A borehole suggests that the near seafloor sediments are composed of  
8 clay-rich nannofossil-foraminiferal ooze and Nannofossil ooze (Wefer et al 1998, Figure 2c).

## 10 **4.2 Seafloor Geomorphology**

11 The seafloor in the study area is situated in water depth ranging between by  $\sim 800 - 2400$  m and is characterized  
12 by a gentle slope of  $\sim 0.9 - 1.5^\circ$  that dips towards the southwest (Figure 5). Different bathymetric features shape  
13 the seafloor such as regions characterized by several depressions and other areas characterized by rough  
14 bathymetric expressions (Figures 5 and 6). The seafloor is divided into two zones: Zone 1 and Zone 2 (Figure 7).

15  
16 Zone 1 occupies the southern portion of the seafloor and accounts for  $\sim 39\%$  of the total study area. It is separated  
17 from Zone 2 by a sharp downcutting seafloor scarp (Figure 7). This zone corresponds to the MTC observed from  
18 the seismic cross sections (Figures 4 and 8). Therefore, we suggest that Zone 2 is formed as a result of mass  
19 wasting events that deformed the present-day seafloor (Figure 7). Although the entire MTC is not fully imaged  
20 by our dataset, we hypothesize the headwall is located upslope in the north and the toe further downslope in the  
21 south. However, parts of the western lateral margin are well imaged as a sharp scarp along the seafloor (Figures  
22 4 and 5).

23  
24 Zone 2 is the focus of this study and accounts for 61% of the total seafloor area. It is characterized by relatively  
25 undeformed areas, which is punctuated by several (sub)circle-like depressions and channel-like troughs (Figures  
26 5, 6 and 7). Careful examination of these depressions reveals heterogeneous morphologies, dimensions, and spatial  
27 distribution (Figures 6 and 7). Based on this and considering the water depth boundary of 1500 m as the interface  
28 between NADW and AAIW, Zone 2 is further subdivided into three subzones: Zone 2a, Zone 2b and Zone 2c  
29 (Figure 7).

## 31 **4.3 Pockmarks, Channel-like depressions, and other Irregular depressions**

### 32 **4.3.1. Zone 2a**

33 Zone 2a is in the south-eastern part of Zone 2 and contains 12 depressions appearing as circular to sub-circular  
34 and crescentic features situated in water depth ranging between 1100 – 1500 m (Figures 5, 6 and 7) (Table 1).  
35 These depressions form two trains, orientated NE-SW with a non-uniform spacing (ranges from 1100 to 4400 m)  
36 between individual depressions. Seismic profiles across these depressions reveal U or V-shaped morphology  
37 (Figures 8 and 9a). Also, most of these depressions are localized above buried depressions interpreted as paleo-  
38 turbidite channels (e.g., Gay et al., 2003, 2006; Pilcher & Argent, 2007; Niyazi et al., 2018; Figure 9a). Likewise,  
39 some of the depressions in this zone develop close to shallow faults (Figures 9a). The depressions in this zone and

1 similar morphotypes in Zone 2b and Zone 2c are interpreted as seafloor pockmarks like those mapped along other  
2 continental margins (Hovland & Judd, 1988; Eruteya et al., 2018; Sun et al., 2011; Palan et al., 2020).

3  
4 Size of the circular pockmarks in this zone range between 663 and 2771 m in diameter and 28 and 131m in depth  
5 (Table 1). However, the crescentic pockmarks are mega-pockmarks (km-scale diameter, see Chen et al., 2015)  
6 and are the largest (diameter) amongst the deepest pockmarks in the study area with diameter and depth ranging  
7 between 2360-2822 m and 115-129 m, respectively (Table 1). The crescentic pockmarks have a gentle slope at  
8 their northern flanks and a steeper slope at their southern flanks, indicating a significant interaction with the  
9 downslope gravity flows or bottom currents (Figures 6a and 9a). Long axis of the pockmarks in this zone strike  
10 differently, however, a dominant NE-SW direction can be observed (Figure 7).

#### 11 12 **4.3.1 Zone 2b**

13 Pockmarks in Zone 2b occur in the central to northern portion of the study area, in water depths ranging between  
14 800 and 1500 m (Figures 5 and 7). They tend to be more isolated and unevenly distributed and are more regular  
15 in shape, appearing with a circular to oval morphology in planform (Figures 6 and 7) (Table 1). The pockmarks  
16 are U – V-shaped in seismic profiles and develop above/close to the buried turbidite channels and  
17 erosional/depositional boundaries (Figures 9b, 10a and 11a). Compared to the pockmarks in Zone 2a, the  
18 pockmarks in this zone are smaller, with a diameter and depth of 306 – 1326 m and 7.23 – 72.86 m, respectively  
19 (Table 1). In addition, the long axes of the pockmarks strike in the NW-SE direction (Figure 7).

#### 20 21 **4.3.2 Zone 2c**

22 In contrast to the previous groups of pockmarks, the depressions in Zone 2c have diverse shapes (Figures 5, 6 and  
23 7). They appear as circular to comet-shaped depressions, elongated depressions, channel-like depressions, or  
24 irregular/scour-like features (Figures 5 and 6). Four circular-oval-shaped pockmarks occur in this zone with  
25 diameters ranging between 617 and 1061 m and depth ranging between 23.52 and 72.86 m (Table 1). The  
26 elongated pockmarks have a diameter ranging between 1813 and 2625m and depth of between 32.62 and 71.34  
27 m (Figures 5 and 6c) (Table 1). These pockmarks are oriented NW - SE (Figures 5, 7c and 7).

28  
29 At least two depressions interpreted as comet-like pockmarks also occur in this zone (Figures 5 and 6c). These  
30 comet-like pockmarks resemble the elongated pockmark, however, are different by having asymmetric shape in  
31 seismic profile and with a narrower tail-like morphology upslope and progressively wider diameter down slope  
32 (Figure 11c). Also, one of these comet-like pockmarks evolved above a buried incision interpreted as a channel  
33 (Figure 11c). In general, pockmarks in this zone strike N-S and have diameter and depth ranging between 947 –  
34 1011 m and 45.54 – 48.57 m respectively (Figure 7) (Table 1).

35  
36 Irregular depressions numbering around five are likewise observed in Zone 2c with difficult to define planiform  
37 outline (Figures 5, 6c and 7). These depressions are interpreted as irregular depressions and likely developed from  
38 activities of bottom current scours (e.g., Duarte et al., 2010). The irregular depressions are dominantly elongated  
39 along the NW-SE direction and have depth up to 50 m (Figures 6c and 7). Lastly, two linear channel-like  
40 morphologies named CL-1 and CL-2 develop in the SW segment of Zone 2c and are very close to the seafloor

1 scarp or lateral margin associated with the deposition of the MTC in Zone 1 (Figure 4 and 6c). CL-1 trends NW-  
2 SE with a length of ~ 5.7 km, a maximum width of ~ 1.9 km and a maximum depth of ~ 60 m (Figure 6c and 7).  
3 On the contrary, CL-2 trends NE-SW and is longer than CL1, with a length of ~ 6.1 km and maximum width of  
4 ~ 1.5 km, reaching a maximum depth of up to 50 m (Figures 6c and 7).

#### 6 **4.4. Morphometric relationship of pockmarks**

7 Morphometric characteristics of the pockmarks in each zone are summarized in Table 1. The 50 pockmarks  
8 measured have an average diameter of 951 m and depth of 38 m. Also, the pockmarks have an average perimeter  
9 and area of 2820 m and 0.79 km<sup>2</sup> respectively. Overall, the pockmarks depth and water depth in the study area do  
10 not show obvious correlation ( $R^2=0.02$ ) (Figure 13a). Following the deepest pockmarks are the crescentic and a  
11 circular pockmark (Figure 13). The pockmark diameter and water depth likewise also does not show correlation  
12 ( $R^2=0.03$ ) (Figure 13b). In contrast, the pockmark area and water depth show moderate positive correlation ( $R^2=$   
13  $0.47$ ) (Figure 13c). Also, there is a moderate positive correlation ( $R^2=0.48$ ) between the pockmark diameter and  
14 depth (Figure 13d). Pockmarks in Zone 2a are the deepest and largest and have a wider range value for both depth  
15 and diameter (Figure 12e). The crescentic pockmarks in this zone represents the deepest and largest pockmarks  
16 (Figure 13). Pockmarks in Zone 2b and Zone 2c display similar range of values for the depth, yet the latter has  
17 wider range for the diameter (Figure 13e).

### 18 **5.0. Discussion**

#### 19 **5.1 Origin of pockmarks and other seafloor depressions**

20 The wide spectrum of morphologies exhibited by the seafloor depressions documented in the study area point  
21 towards different genetic mechanisms (Figure 6). Clearly, evolution of these depressions is associated with the  
22 removal of some seafloor sediments, up to a maximum depth of 130 m below the present-day seafloor in the case  
23 of the largest depression (Figure 9a). Lithological examination of the nearest ODP Leg 175 borehole 1087A,  
24 approximately 70 km from the perimeter of the study area, reveals the first 150 m of cored slope sediment is  
25 predominantly composed of clay-rich nannofossil-foraminiferal ooze and nannofossil ooze (Wefer et al 1998;  
26 Figure 2c). Also, majority of the depressions classified as pockmarks are located above potential fluid flow  
27 elements that may allow fluid focusing towards the seafloor, such as buried turbidite channel system, erosional  
28 flanks and faults (e.g. Gay et al., 2003, 2006; Cartwright et al., 2007; Pilcher & Argent, 2007; Sun et al., 2011;  
29 Figures 8-11). Therefore, we consider the pockmarks to have developed from the expulsion of fluids and fluidized  
30 sediments along the seafloor, within the predominantly fine-grained seafloor sediments (Judd & Hovland, 2007;  
31 Hovland et al., 2010). This mechanism is generally accepted as the origin of the circular depressions classified as  
32 pockmarks along continental margins irrespective of their configuration, dimensions, and sizes (Hovland, Gardner  
33 & Judd, 2002; Judd & Hovland, 2007; Pilcher & Argent, 2007; Andresen, Huuse & Clausen, 2008). Similar  
34 seafloor features have been mapped in other parts of the Orange Basin (Hartwig et al. 2012; Palan et al., 2020;  
35 Mahlalela et al., 2021) and along other continental margins worldwide where they have been identified as  
36 pockmarks (Hovland & Judd, 1988; Sun et al., 2011; Eruteya et al., 2018; Omeru et al., 2021). The occurrence  
37 of these pockmarks along continental margins is usually evidence for either past or current migration/leakage of  
38 fluids from subsurface reservoirs and the presence of an active petroleum system (Heggland, 1998; Andresen et

1 al., 2021). However, in the case of the present study area, the lack of geochemical and flare information from  
2 these pockmarks does not permit commenting further on any ongoing fluid seepage activities.

3  
4 Pockmarks evolve primitively as circular seafloor morphologies (Bøe et al., 1998; Hovland et al., 2002; Andresen  
5 et al., 2008). Therefore, the crescentic, elongated and comet pockmarks mapped on the seafloor require seafloor  
6 processes postdating the original pockmark formation (Sun et al., 2011; Chen et al., 2015; Palan et al., 2020,  
7 Figures 6 and 7). Hovland et al. (2002) concluded that elongation of pockmarks occurs in areas influenced by  
8 bottom currents that are capable of reshaping the pockmark morphology. Consequently, we suggest that the  
9 oceanographic activities in the study area associated with strong bottom currents are important processes that can  
10 sculpt the seafloor and pre-existing seafloor morphologies, creating both erosional and depositional morphologies  
11 (e.g., Masson et al., 2004, Sayago-Gil et al., 2010; Schattner et al., 2016). The seafloor in the present study area  
12 lies within a water depth of 800 - 2400 m, which coincides with the depth of influence of two counter-currents,  
13 the Antarctic Intermediate Water (AAIW) and North Atlantic Deep Water (NADW) oceanic currents (Weigelt  
14 and Uenzelmann-Neben, 2004; Figures 1 and 7). These currents circulate the SW African margin at different  
15 depths impinging the different seafloor zones along the slope as classified in the present study area (Figure 7).  
16 The north-westerly flowing AAIW prevailing at a water depth of 500 - 1500 m, which covers pockmarks in Zone  
17 2a and Zone 2b.

18  
19 However, it is likely that the AAIW has a limited influence on the morphology of pockmarks in these zones. An  
20 interesting observation in our study is that the majority of the pockmarks (n=9) in Zone 2a are elongated along  
21 the NNW-SSW direction, with some exception (n=3) that have long axis striking E-W direction (Figure 7).  
22 Josenhans et al. (1978) suggested that Unidirectional currents could unevenly modify the geometry of the  
23 pockmarks, and downslope pockmark sidewall is more prone to the erosion or non-deposition compared to the  
24 upslope sidewall. This means that the initial circular shaped pockmarks can be elongated along the current  
25 direction. The slope gradient for Zone 2a is along NNW-SSW direction (Figure 7), thus, suggesting that the  
26 downslope current may have reshaped the NNW-SSW elongated pockmarks. In seismic cross section, these  
27 pockmarks have steeper upslope sidewall than downslope (Figure 8a), further strengthening the interpretation of  
28 downdip elongation of pockmark by the downslope current erosion. In comparison, the E-W elongated crescentic  
29 pockmarks in Zone 2a is likely influenced by the AAIW bottom current activity (Figures 5 and 6). This  
30 perpendicular elongation of seafloor depressions relative to the current direction has been observed along the  
31 Northern Orange Basin, offshore Namibia (Wenau et al., 2021). This interplay of erosion and deposition may have  
32 led to a lateral elongation of the pockmark normal to the current direction. Pockmarks reshaped by activities of  
33 bottom currents are also documented in the northern (Mahlalela et al., 2021) and southern segment of the Orange  
34 Basin, offshore South Africa (Palan et al., 2020). In addition, worth considering is the hypothesis that these  
35 crescentic pockmarks here may have likewise evolved from the coalescing of multiple pockmarks based on the  
36 close spacing and linear arrangement of the pockmark in Zone 2a (Figure 6a). This would have been promoted by  
37 the combined action of fluid escape and bottom current activities resulting in the crescentic morphology (cf.  
38 Hovland et al., 2002). On the contrary, the long axis of the pockmarks in Zone 2b is dominantly parallel to the  
39 slope gradient (Figures 7 and 9b), suggesting a similar mechanism with the majority of the pockmarks in Zone 2a  
40 that are developed by the modification of downslope current. However, it is interesting that the crescentic

1 pockmarks are only observed in the Zone 2a, but not in Zone 2b, which is under the dominance of the same AAIW.  
2 We speculate that the dramatic changes in water depth from Zone 1 to Zone 2a may have strengthened the bottom  
3 current activity, which contributed the formation of the crescentic pockmarks in Zone 2a. While the relatively low  
4 slope gradient may have weakened the AAIW and together with the sparse pockmark distribution, disfavoured  
5 the formation of crescentic pockmarks in Zone 2b.

6  
7 However, the underlying south easterly flowing NADW currents with a depth of influence of 1500 - 4000 m may  
8 impact greatly the morphology of pockmarks and other classes of depressions in Zone 2c (Figures 5-7). The  
9 comet-shaped pockmarks and one of elongated pockmarks exhibiting a NW-SE elongation is in good agreement  
10 with NW-SE flow direction of the NADW current (Figures 1, 6 and 7). Therefore, these comet-like pockmarks  
11 may have firstly developed from fluid expulsion along the seafloor and subsequently modified by the NADW  
12 currents. Similar origin has been invoked for the evolution of comet-like depression along the Zambezi margin,  
13 offshore Mozambique (Deville et al., 2020).

14  
15 On the other hand, the channel-like depressions (CL1 and CL2) occurring in Zone 2c may have evolved in two  
16 possible ways based on their morphology and different orientation on the seafloor (Figures 6 and 7). Firstly,  
17 possibly from the amalgamation of single pockmarks (Hovland, Gardner & Judd, 2002) or elongated pockmarks  
18 having a similar orientation for their long axis (Sun et al., 2011). This is based on the observation of localized  
19 deeper segments within these channel-like depressions (Figures 6c). Especially in the case of CL2 the NADW  
20 bottom current may have further shaped and connected this string of pockmarks since this region is already  
21 compromised in terms of geotechnical integrity arising from subsurface focused fluid flow activities. However,  
22 these channel-like depressions, especially may represent immature channels created simply by turbidity currents  
23 in the study area (e.g., Sun et al., 2011).

24  
25 The other intricate depressions in Zone 2c described as irregular depression exhibit a poorly defined and closed  
26 perimeter/boundary in plain view suggested a complicated evolution (Figure 6c). We hypothesis these irregular  
27 depressions developed from the opportunistic removal or winnowing of sediments from pre-existing depressions  
28 or pockmarks along the seafloor either by slumping or simply by the complex NADW current flow winnowing  
29 sediments within this section of the seafloor.

## 30 **5.2. Controls on the spatial distribution and size of the pockmarks in the study area**

31 Pockmarks identified in the study area are non-randomly distributed on the seafloor (Figures 5-7). The spatial  
32 distribution of these pockmarks is related to the structural and stratigraphic organization along this section of the  
33 slope associated with deepwater gravity-flow and palaeoceanographic processes in the study area (Figures 5 and  
34 7). The variance horizon probe 100 ms TWT below the seafloor revealed a complex subsurface architecture  
35 encompassing a region of paleo-channel incisions and regions of MTCs and deepwater lobes (Figure 12). Over  
36 90% of the pockmarks across all zones in the study area exhibit a preferential seafloor alignment in relation to the  
37 axis of buried turbidite channels. These channels drain southwards, matching the alignment and spatial distribution  
38 of the pockmarks on the seafloor (compare Figure 12 a and b). This observation is not unique, as similar alignment  
39 of pockmarks above paleochannels has been documented along the West African margin (Gay et al., 2003, 2006;  
40

1 Pilcher & Argent, 2007) and in the Zhongjiannan Basin, South China Sea (Chen et al., 2018). Here, the turbidite  
2 channel systems may serve as conduits for storing and redistributing fluids in the subsurface, which are later  
3 focused on the seafloor for expulsion. However, the storage capacity of these channels is dictated by the  
4 lithological nature of their infill, which modulates fluid flow within these channels (Gay et al., 2003). In a scenario  
5 where these channels are coarse grain dominated, they represent preferred subsurface pathways for fluid migration  
6 and focusing towards the seafloor (Pilcher & Argent, 2007). The development of these turbidite channels in some  
7 instances near shallow faults may suggest these paleochannels serve as transient reservoirs and conduits for storing  
8 fluid in the shallow reservoir within Neogene sediments (Figure 9). Similarly, in offshore Niger Delta, alignment  
9 of non-random pockmarks is related to the internally deformed areas of buried mass transport deposits, suggesting  
10 a linkage between submarine mass wasting and subsurface fluid migration (Riboulot et al., 2013). These deformed  
11 regions in the subsurface represent ideal pathways for preferential channelling of fluids. We invoke similar  
12 processes for localising some of the pockmarks above regions internally deformed parts and outline of MTCs and  
13 other buried erosional flanks and in the study area (Figures 9b and 10c).

14

15 The diameter and depth of the pockmarks in the study area fall within an expected range comparing to those  
16 previously reported pockmarks around the world yet representing one of the largest and deepest pockmarks  
17 (Pilcher and Argent, 2007) (Figure 13f). Generally, a moderate positive correlation exists between the pockmark  
18 morphometry parameter examined (Figure 13).

19 Importantly, the positive correlation between the pockmark diameter and pockmark depth documented in this  
20 study also exists for pockmarks characterized e.g., offshore western Indian (Dandapath et al., 2010), offshore  
21 Niger-Delta (Omeru et al., 2021), and in Belfast, Bay (Andrews et al., 2010). Pockmarks in Zone 2a appear to be  
22 relatively larger and deeper than those documented across Zone 2b and Zone 2c (Figures 4 and 12 and Table 1).  
23 Factors controlling the size of pockmarks developed on the seafloor in the study include the volume of fluids  
24 available for pockmark formation (Judd and Hovland, 2007). This is related to the size of the reservoirs, depth to  
25 fluid source/reservoir (e.g. Roelofse et al. 2020) and bottom current sculpting activities in the study area.  
26 Following, larger volume of fluids accumulated in subsurface reservoirs for e.g., in this case the underlying  
27 channels controlling the pockmark distribution or contourite deposits in the overburden as is the case of the present  
28 study area, the larger the overpressure generated. This would eventually result in the formation of larger  
29 pockmarks arising from the expulsion of greater quantities of fluids and fluidized sediments on the seafloor.  
30 Qualitative examinations of buried turbidite channels underlying the pockmark in Zone 2a reveal a larger channel  
31 width and depth than those of the smaller channels underlying the pockmarks in Zone 2b and Zone 2c (Figure 12).  
32 Therefore, these larger channels will have higher storage capacity (volume) and larger surface area for focusing  
33 fluid towards the seafloor for expulsion resulting in larger pockmarks in Zone 2a compared to those other zones  
34 with smaller channels (Figure 12). A critical factor controlling pockmark size is the nature of the sediments  
35 (lithology) and thickness of sediments in which the pockmarks develop and (Hovland et al. 1984). Possible lateral  
36 heterogeneity in the lithology of the study area may drive the non-uniformity of the pockmark size. Another  
37 control on the size of the pockmark relating to the bottom current circulation is already discussed under Section  
38 5.1. as responsible for the development of the crescentic pockmarks.

39

1 Notably, the source of fluids driving pockmark formation affects the size of the pockmarks in two ways. A deep  
2 source of fluids will require a more tremendous fluid pressure to overcome the sealing integrity of the overburden  
3 (Roelofse et al. 2020). Gas expansion and pore pressure increase occur in the subsurface as gas migrates towards  
4 the seafloor, where it results in pockmark formation (Judd & Hovland 2007). However, a shallower fluid source  
5 may still form a large pockmark if the volume of fluids is substantial (Roelofse et al. 2020).

#### 7 **5.4. Potential source(s) of fluids driving the evolution of pockmarks in the study area**

8 Based on the tectonostratigraphic organization of the study area (Figures 2 and 3), two potential fluid sources  
9 exist: a shallow and a deeper fluid source, capable of driving the formation of the seafloor pockmarks.

##### 11 **5.4.1 Deep fluid source**

12 The Albian/Aptian source rocks are well documented as the key source for thermogenic gas in the Orange Basin  
13 (e.g., Brown, 1995; Jungslager 1999; Van Der Spuy 2003; Hartwig et al. 2012). In fact, the gas and condensate  
14 produced from Ibhubesi and Kudu fields in the northern Orange Basin are derived from the Lower Aptian Black  
15 Shales (Bray et al. 1998; van der Spuy 2003) (Figures 1 and 2a). Unfortunately, the 3D seismic dataset interpreted  
16 in the study area was cut at the Cenomanian-Turonian level, and the Lower Aptian Interval was not imaged (Figure  
17 7). The Cenomanian-Turonian organic-rich shales represent another potential deep fluid source in the Orange  
18 Basin (e.g., Jungslager 1999; Aldrich et al. 2003; Van Der Spuy 2003; Hartwig et al. 2012). Some localized fluid-  
19 based amplitude anomalies such as bright spots discovered in the compartmentalized compressional domain of  
20 the Late Cretaceous Mega Slide Complex detaching above the Cenomanian-Turonian source rocks point towards  
21 storage and trapping of hydrocarbons derived from underlying source rocks these deep source rocks (Figure 7).

22  
23 We likewise invoke this fluid source as capable of driving the formation of the seafloor pockmarks in this segment  
24 of the Orange Basin. Thermogenic or deeper-sourced gas is transported upward along the fault complex associated  
25 with the Late Cretaceous Megaslide complex into the shallower overburden (Hartwig et al., 2012, Mahlalela et  
26 al., 2021) (Figures 8 and 10). These fluids can then be stored and redistributed in shallow potential reservoirs  
27 (Figures 8 and 10).

##### 29 **5.4.2 Shallow fluid sources**

30 Possible shallow fluid flow sources identified in the study area include the contourite deposits and the turbidite  
31 channel systems in the uppermost Paleogene sediments (Figures 7-10). The contourite deposits in the study area  
32 may act as seals or reservoirs depending on their lithological composition. If these contourite deposits are  
33 composed of fine-grained sediments, they may act as seals, while those containing coarse-grained sediments  
34 represent potential reservoirs (Rebesco et al. 2014). Contourite reservoirs have been documented in the Santos  
35 Basin, offshore Brazil (Viana 2008), the North Sea (Enjolras et al. 1986) and the Strait of Gibraltar (León et al.  
36 2014). However, bottom current-derived deposits are mixed in composition (Stow et al., 2008) and may form  
37 reservoirs with varying petrophysical properties. For example, contourite drifts in the Gulf of Cádiz are  
38 characterized by the alternation of low-permeability (fine-grained sediments) and high permeability (coarse  
39 sediments) layers (Faugères & Mulder 2011).

1 It is likely the contourite deposits do not contain hydrocarbons and are entirely pore-water laden. Rapid loading  
2 of these contourite deposits promotes overpressure generation and expulsion of fluids via dewatering (Rebesco &  
3 Camerlenghi 2008). Importantly the connection between the contourite deposits and deeply rooted faults suggest  
4 these contourite deposits may trap hydrocarbon gas generated from the deep source rocks and transported upward  
5 along the faults (Figures 8a and 11a). The presence of fluid-based amplitude anomalies associated within some of  
6 these deposits suggests the presence of shallow gas (e.g., Andreassen et al., 2007; Figure 11a).

7  
8 The buried turbidite channel systems in the study area can either be the source of shallow gas or may act as  
9 reservoirs for storing fluids. The channels can act as conduits for fluid migration and redistribution within the  
10 subsurface when the infill is coarse grain dominated (Pilcher & Argent 2007). Also, microbial gas may be  
11 generated via microbial decomposition within sediments buried within these channels if the sediments are organic-  
12 rich (Dickens et al., 2004). Abundant biogenic gases were encountered in the near seafloor sediments at ODP Site  
13 1087, pointing towards the presence of suitable microbial communities in this area (Wefer et al., 1998; Figure 1).  
14 In addition, high total gas pressure was encountered in sediments at site 1087 between 15 - 200 m below the  
15 seafloor (Wefer et al., 1998). These channels may also trap deeper thermogenic hydrocarbons where a viable fluid  
16 migration pathway afforded by fault systems associated with Late Cretaceous Mega Slide Complex connect the  
17 shallower basin stratigraphy (Figure 10a).

## 19 **5.5. Conceptual model for the evolution of pockmarks in the study area**

20 Following the discussion above, we propose a conceptual fluid flow model driving pockmark formation along this  
21 segment of the Orange Basin in Figure 14a. A dual fluid source is favoured where deep hydrocarbons are sourced  
22 from Cretaceous source rocks (either the Albian/Aptian source rock or Cenomanian-Turonian source rocks) and  
23 channelled along complex faults associated with the megaslide complex into the shallower overburden. This fluid  
24 may be mixed with biogenic fluid from the shallow source(s) originating from the buried channels or contourite  
25 deposits (Figure 14a). The upward migrating gas from deeper intervals can be stored and redistributed in the  
26 contourites or channel systems where variable lithological facies exist. Supporting this is the presence of  
27 amplitude anomalies diagnostic of shallow gas in shallow sediments (Figures 10a and 11a). Otherwise, the fluid  
28 accumulated in the near seafloor domain is essentially biogenic gases trapped in the buried channels with no  
29 contribution from the deep source rocks. The accumulated fluids in channels and within other porous sediments  
30 in the near seafloor domain generate excess pore pressure (Figure 14a and 14b Stage 1). Subsequently, the  
31 pockmarks developed from the expulsion of overpressured fluids and fluidized sediments along the seafloor  
32 (Figure 14b Stage 2). Finally, bottom current circulation involving the Antarctic Intermediate Water (AAIW),  
33 North Atlantic Deep Water (NADW) and along slope current in the study area resulted in the modification of the  
34 initial pockmark morphology, resulting in other end-member series such as crescentic, elongated and comet  
35 pockmarks and other irregular depressions mapped along the seafloor in this deepwater segment of the northern  
36 Orange Basin (Figure 14b Stage 3).

37

## 1 **5.6. Implications on deepwater geohazard assessment and hydrocarbon exploration in the Northern Orange** 2 **Basin**

3 Hydrocarbon exploration activities in recent times have transited into deep waters in the Orange Basin (Sallomo,  
4 2012) as they have along other margins (Alves et al., 2014). Identifying subsurface fluid migration systems is vital  
5 for hydrocarbon exploration and prospect risk analysis in deepwater. Therefore, the discovery of these pockmarks  
6 and other intricate depressions on the seafloor in this deepwater segment has implications on hydrocarbon  
7 exploration related to both (a) deepwater geohazards and (b) economics, in the light of depletion of prospective  
8 deeper reservoirs.

9 Geohazards to hydrocarbon exploration are usually screened for up to 1 sec TWT (or ~750 m) below the seafloor  
10 and encompasses some of the features documented in study area such as pockmarks, channel-like morphologies,  
11 MTCs, faults and shallow gas (e.g., Sharp & Samuel, 2004; Sharp & Badalini, 2013; Figures 8 and 10). The  
12 likelihood of remnant fluids in the buried channels and other regions with localized pockets of shallow gas in the  
13 overburden may represent deepwater geohazards while drilling through the overburden in the study area. The  
14 spatial distribution of the pockmarks on the seafloor will affect decisions relating to well placement and  
15 localization of subsea infrastructure in this area (Figure 5). Therefore, such geohazards must be considered when  
16 planning exploration and infrastructure installation activities in this area.

17 Manifestations of fluid flow and escape features in the study area suggest the occurrence of a deeper reservoir  
18 (Heggland, 1998). Therefore, these features and potential secondary migration pathways in the overburden should  
19 be included in petroleum system modelling exercises for the study area to quantify the volume of hydrocarbon  
20 vented along the seafloor and those remaining in the reservoir. This is necessary to derisk prospects and determine  
21 their economic viability.

## 22 23 **6.0. Conclusions**

24 This study characterized 50 present-day seafloor pockmarks, several irregular depressions and channel-like  
25 morphologies along the slope of the Northern Orange Basin, offshore South-Africa using high-quality 3D seismic  
26 survey. The majority of these pockmarks display elongated, crescentic or comet-shaped, suggesting evidence of  
27 post-formation modification by the action of bottom currents. Clearly, these pockmarks are non-randomly  
28 developed. Based on the spatial distribution of these pockmarks above an underlying turbidite channel system, we  
29 suggest a genetic link where fluids are focused within this structure for expulsion along the seafloor. Importantly,  
30 this study emphasizes the role of shallow reservoirs in the Orange Basin, such as channels and contourite deposits  
31 as vital components of the fluid plumbing system along the slope. This new evidence of fluid escape along the  
32 Orange Basin may suggest similar fluid escape structures may be more pervasive than currently documented along  
33 these sections of the eastern South Atlantic Ocean. In all, the mechanism proposed here for the formation of  
34 pockmarks may be applicable to other margins that are hydrocarbon-rich and have experienced multiple episodes  
35 of slope instabilities coupled with strong oceanographic influences.

36  
37  
38

## 1   **References**

- 2   Alves, T. M., Bell, R. E., Jackson, C. L., & Minshull, T. A. (2014). Deep-water continental margins: geological  
3   and economic frontiers. *Basin Research*, 26(1), 3-9.
- 4   Andreassen, K., Nilssen, E. G., & Ødegaard, C. M. (2007). Analysis of shallow gas and fluid migration within the  
5   Plio-Pleistocene sedimentary succession of the SW Barents Sea continental margin using 3D seismic data. *Geo-*  
6   *Marine Letters*, 27(2), 155-171.
- 7   Andresen, K. J. (2012). Fluid flow features in hydrocarbon plumbing systems: What do they tell us about the basin  
8   evolution? *Marine Geology*, 332, 89-108.
- 9   Andresen, K. J. et al. (2021) 'The longevity of pockmarks – A case study from a shallow water body in northern  
10   Denmark', *Marine geology*, 434, p. 106440. doi: 10.1016/j.margeo.2021.106440.
- 11   Andresen, K. J., & Huuse, M. (2011). 'Bulls-eye' pockmarks and polygonal faulting in the Lower Congo Basin:  
12   Relative timing and implications for fluid expulsion during shallow burial. *Marine Geology*, 279(1-4), 111-127.
- 13   Andresen, K. J., Huuse, M., & Clausen, O. R. (2008). Morphology and distribution of Oligocene and Miocene  
14   pockmarks in the Danish North Sea—implications for bottom current activity and fluid migration. *Basin Research*,  
15   20(3), 445-466.
- 16   Andrews, B. D., Brothers, L. L., & Barnhardt, W. A. (2010). Automated feature extraction and spatial organization  
17   of seafloor pockmarks, Belfast Bay, Maine, USA. *Geomorphology*, 124(1-2), 55-64.
- 18   Berndt, C. (2005). Focused fluid flow in passive continental margins. *Philosophical Transactions of the Royal*  
19   *Society A: Mathematical, Physical and Engineering Sciences*, 363(1837), 2855-2871.
- 20   Bøe, R., Rise, L., & Ottesen, D. (1998). Elongate depressions on the southern slope of the Norwegian Trench  
21   (Skagerrak): morphology and evolution. *Marine Geology*, 146(1-4), 191-203.
- 22   Bray, R., Lawrence, S., & Swart, R. (1998). Source rock, maturity data indicate potential off Namibia. *Oil and*  
23   *Gas Journal*, 96(32), 84-88.
- 24   Brown, L. F. (Ed.). (1995). *Sequence Stratigraphy in Offshore South African Divergent Basins: An Atlas on*  
25   *Exploration for Cretaceous Lowstand Traps by Soekor (Pty) Ltd, AAPG Studies in Geology 41* (No. 41). AAPG.
- 26   Bull, S., Cartwright, J., & Huuse, M. (2009). A review of kinematic indicators from mass-transport complexes  
27   using 3D seismic data. *Marine and Petroleum Geology*, 26(7), 1132-1151.
- 28   Cartwright, J., Huuse, M., & Aplin, A. (2007). Seal bypass systems. *AAPG bulletin*, 91(8), 1141-1166.
- 29   Chen, J., Song, H., Guan, Y., Pinheiro, L. M., & Geng, M. (2018). Geological and oceanographic controls on  
30   seabed fluid escape structures in the northern Zhongjiannan Basin, South China Sea. *Journal of Asian Earth*  
31   *Sciences*, 168, 38-47.

- 1 Chen, J., Song, H., Guan, Y., Yang, S., Pinheiro, L. M., Bai, Y., ... & Geng, M. (2015). Morphologies,  
2 classification and genesis of pockmarks, mud volcanoes and associated fluid escape features in the northern  
3 Zhongjiannan Basin, South China Sea. *Deep Sea Research Part II: Topical Studies in Oceanography*, 122, 106-  
4 117.
- 5 Dalton, T. J. S., Paton, D. A., & Needham, D. T. (2017). Influence of mechanical stratigraphy on multi-layer  
6 gravity collapse structures: insights from the Orange Basin, South Africa. *Geological Society, London, Special  
7 Publications*, 438(1), 211-228.
- 8 Dandapath, S., Chakraborty, B., Karisiddaiah, S. M., Menezes, A., Ranade, G., Fernandes, W., ... & Raju, K. P.  
9 (2010). Morphology of pockmarks along the western continental margin of India: employing multibeam  
10 bathymetry and backscatter data. *Marine and Petroleum Geology*, 27(10), 2107-2117.
- 11 de Vera, J., Granado, P., & McClay, K. (2010). Structural evolution of the Orange Basin gravity-driven system,  
12 offshore Namibia. *Marine and Petroleum Geology*, 27(1), 223-237.
- 13 Deville, E., Scalabrin, C., Jouet, G., Cattaneo, A., Battani, A., Noirez, S., ... & Loubrieu, B. (2020). Fluid seepage  
14 associated with slope destabilization along the Zambezi margin (Mozambique). *Marine Geology*, 428, 106275.
- 15 Dickens, A. F., Gelinas, Y., Masiello, C. A., Wakeham, S., & Hedges, J. I. (2004). Reburial of fossil organic  
16 carbon in marine sediments. *Nature*, 427(6972), 336-339.
- 17 Dingle, R. V., & Scrutton, R. A. (1974). Continental breakup and the development of post-Paleozoic sedimentary  
18 basins around southern Africa. *Geological Society of America Bulletin*, 85(9), 1467-1474.
- 19 Duarte, J. C., Terrinha, P., Rosas, F. M., Valadares, V., Pinheiro, L. M., Matias, L., ... & Roque, C. (2010).  
20 Crescent-shaped morphotectonic features in the Gulf of Cadiz (offshore SW Iberia). *Marine Geology*, 271(3-4),  
21 236-249.
- 22 Enjolras, J. M., Gouadain, J., Mutti, E., & Pizon, J. (1986). New turbiditic model for the Lower Tertiary sands in  
23 the South Viking Graben. In *Habitat of hydrocarbons on the Norwegian continental shelf. International conference*  
24 (pp. 171-178).
- 25 Eruteya, O. E., Niyazi, Y., Omosanya, K. O., Ierodiaconou, D., & Moscariello, A. (2020). Evolution and  
26 morphology of rafted blocks in an ancient deepwater mass-transport complex (Exmouth Plateau, offshore North  
27 West Australia). *Interpretation*, 8(4), SV31-SV50.
- 28 Eruteya, O. E., Reshef, M., Ben-Avraham, Z., & Waldmann, N. (2018). Gas escape along the Palmachim  
29 disturbance in the Levant Basin, offshore Israel. *Marine and Petroleum Geology*, 92, 868-879.
- 30 Eruteya, O. E., Safadi, M., Waldmann, N., Makovsky, Y., & Ben-Avraham, Z. (2016). Seismic geomorphology  
31 of the Israel slump complex in the Levant basin (SE Mediterranean). In *Submarine mass movements and their  
32 consequences* (pp. 39-47). Springer, Cham.

- 1 Faugères, J. C., & Mulder, T. (2011). Contour currents and contourite drifts. In *Developments in Sedimentology*  
2 (Vol. 63, pp. 149-214). Elsevier.
- 3 Frey-Martinez, J., Cartwright, J., & Hall, B. (2005). 3D seismic interpretation of slump complexes: examples from  
4 the continental margin of Israel. *Basin Research*, 17(1), 83-108.
- 5 Gadol, O., Tibor, G., ten Brink, U., Hall, J. K., Groves-Gidney, G., Bar-Am, G., ... & Makovsky, Y. (2020). Semi-  
6 automated bathymetric spectral decomposition delineates the impact of mass wasting on the morphological  
7 evolution of the continental slope, offshore Israel. *Basin Research*, 32(5), 1166-1193.
- 8 Gafeira, J., Long, D., & Diaz-Doce, D. (2012). Semi-automated characterisation of seabed pockmarks in the  
9 central North Sea. *Near Surface Geophysics*, 10(4), 301-312.
- 10 Gay, A., Lopez, M., Berndt, C., & Seranne, M. (2007). Geological controls on focused fluid flow associated with  
11 seafloor seeps in the Lower Congo Basin. *Marine Geology*, 244(1-4), 68-92.
- 12 Gay, A., Lopez, M., Cochonat, P., Séranne, M., Levaché, D., & Sermondadaz, G. (2006). Isolated seafloor  
13 pockmarks linked to BSRs, fluid chimneys, polygonal faults and stacked Oligocene–Miocene turbiditic  
14 palaeochannels in the Lower Congo Basin. *Marine Geology*, 226(1-2), 25-40.
- 15 Gay, A., Lopez, M., Cochonat, P., Sultan, N., Cauquil, E., & Brigaud, F. (2003). Sinuous pockmark belt as  
16 indicator of a shallow buried turbiditic channel on the lower slope of the Congo Basin, West African Margin.  
17 *Geological Society, London, Special Publications*, 216(1), 173-189.
- 18 Gerrard, I., & Smith, G. C. (1982). Post-Paleozoic Succession and Structure of the Southwestern African  
19 Continental Margin: Rifted Margins: Field Investigations of Margin Structure and Stratigraphy.
- 20 Hartwig, A., Anka, Z., & di Primio, R. (2012). Evidence of a widespread paleo-pockmarked field in the Orange  
21 Basin: An indication of an early Eocene massive fluid escape event offshore South Africa. *Marine Geology*, 332,  
22 222-234.
- 23 Hartwig, A., Anka, Z., & di Primio, R. (2012). Evidence of a widespread paleo-pockmarked field in the Orange  
24 Basin: An indication of an early Eocene massive fluid escape event offshore South Africa. *Marine Geology*, 332,  
25 222-234.
- 26 Heggland, R. (1998). Gas seepage as an indicator of deeper prospective reservoirs. A study based on exploration  
27 3D seismic data. *Marine and Petroleum Geology*, 15(1), 1-9.
- 28 Hovland, M., & Judd, A. G. (1988). *Seabed pockmarks and seepages: impact on geology, biology, and the marine*  
29 *environment*. Graham & Trotman.
- 30 Hovland, M., Gardner, J. V., & Judd, A. G. (2002). The significance of pockmarks to understanding fluid flow  
31 processes and geohazards. *Geofluids*, 2(2), 127-136.

- 1 Hovland, M., Hegglund, R., De Vries, M. H., & Tjelta, T. I. (2010). Unit-pockmarks and their potential  
2 significance for predicting fluid flow. *Marine and Petroleum Geology*, 27(6), 1190-1199.
- 3 Isiaka, A. I., Durrheim, R. J., Manzi, M. S., & Andreoli, M. A. (2017). 3D seismic analysis of the AK Fault,  
4 Orange Basin, South Africa: Implications for hydrocarbon leakage and offshore neotectonics. *Tectonophysics*,  
5 721, 477-490.
- 6 Josenhans, H. W., King, L. H., & Fader, G. B. (1978). A side-scan sonar mosaic of pockmarks on the Scotian  
7 Shelf. *Canadian Journal of Earth Sciences*, 15(5), 831-840.
- 8 Judd, A., & Hovland, M. (2007). *Seabed fluid flow: the impact on geology, biology and the marine environment*.  
9 Cambridge University Press.
- 10 Judd, A., & Hovland, M. (2009). *Seabed fluid flow: the impact on geology, biology and the marine environment*.  
11 Cambridge University Press.
- 12 Jungslager, E. H. (1999). *Petroleum habitats of the Atlantic margin of South Africa*. Geological Society, London,  
13 Special Publications, 153(1), 153-168.
- 14 Karaket, A., Chenrai, P., & Huuse, M. (2021). Seismic Characteristics of Paleo-Pockmarks in the Great South  
15 Basin, New Zealand. *Frontiers in Earth Science*, NA-NA.
- 16 Kuhlmann, G., Adams, S., Campher, C., van der Spuy, D., di Primio, R., & Horsfield, B. (2010). Passive margin  
17 evolution and its controls on natural gas leakage in the southern Orange Basin, blocks 3/4, offshore South Africa.  
18 *Marine and Petroleum Geology*, 27(4), 973-992.
- 19 Kumar, P. C., Alves, T. M., & Sain, K. (2021). Submarine canyon systems focusing sub-surface fluid in the  
20 Canterbury Basin, South Island, New Zealand. *Scientific Reports*, 11(1), 1-16.
- 21 León, R., Somoza, L., Medialdea, T., González, F. J., Gimenez-Moreno, C. J., & Pérez-López, R. (2014).  
22 Pockmarks on either side of the Strait of Gibraltar: formation from overpressured shallow contourite gas reservoirs  
23 and internal wave action during the last glacial sea-level lowstand?. *Geo-Marine Letters*, 34(2-3), 131-151.
- 24 Macdonald, D., Gomez-Perez, I., Franzese, J., Spalletti, L., Lawver, L., Gahagan, L., ... & Paton, D. (2003).  
25 Mesozoic break-up of SW Gondwana: implications for regional hydrocarbon potential of the southern South  
26 Atlantic. *Marine and Petroleum Geology*, 20(3-4), 287-308.
- 27 Mahlalela, V., Manzi, M. S. D., Jinnah, Z., Bourdeau, J. E., & Durrheim, R. J. (2021). Structural characteristics  
28 and 3D seismic detection of gas migration pathways in the deep-water Orange Basin, South Africa. *Marine*  
29 *Geophysical Research*, 42(1), 1-17.
- 30 Masson, D. G., Wynn, R. B., & Bett, B. J. (2004). Sedimentary environment of the Faroe-Shetland and Faroe  
31 Bank Channels, north-east Atlantic, and the use of bedforms as indicators of bottom current velocity in the deep  
32 ocean. *Sedimentology*, 51(6), 1207-1241.

- 1 Niyazi, Y., Eruteya, O. E., Harishidayat, D., Johansen, S. E., & Waldmann, N. (2018). Seismic geomorphology  
2 of submarine channel-belt complexes in the Pliocene of the Levant Basin, offshore central Israel. *Marine Geology*,  
3 403, 123-138.
- 4 Niyazi, Y., Eruteya, O. E., Warne, M., & Ierodiaconou, D. (2021). Discovery of large-scale buried volcanoes  
5 within the Cenozoic succession of the Prawn Platform, offshore Otway Basin, southeastern Australia. *Marine and*  
6 *Petroleum Geology*, 123, 104747.
- 7 Nürnberg, D., & Müller, R. D. (1991). The tectonic evolution of the South Atlantic from Late Jurassic to present.  
8 *Tectonophysics*, 191(1-2), 27-53.
- 9 Omeru, T., Ayerume, D., Bankole, S., Ogbe, O. B., Byami, J. A., Obafemi, S., ... & Pat-Nebe, O. C. (2021).  
10 Geomorphometric analysis of seabed pockmarks, offshore western Niger Delta: A case study of the Freeman  
11 Field. *Interpretation*, 9(2), T569-T584.
- 12 Ostanin, I., Anka, Z., di Primio, R., & Bernal, A. (2013). Hydrocarbon plumbing systems above the Snøhvit gas  
13 field: structural control and implications for thermogenic methane leakage in the Hammerfest Basin, SW Barents  
14 Sea. *Marine and Petroleum Geology*, 43, 127-146.
- 15 Palan, K., Green, A. N., Andrews, B., Sink, K., & Wiles, E. A. (2020). A morphometric analysis of the fluid flow  
16 features of the southern Orange Basin, South Africa. *Marine Geology*, 423, 106145.
- 17 Partridge, TC & Maud, R. R. (1987). Geomorphic evolution of southern Africa since the Mesozoic. *South African*  
18 *Journal of Geology*, 90(2), 179-208.
- 19 Paton, D. A., Di Primio, R., Kuhlmann, G., Van Der Spuy, D., & Horsfield, B. (2007). Insights into the petroleum  
20 system evolution of the southern Orange Basin, South Africa. *South African Journal of Geology*, 110(2-3), 261-  
21 274.
- 22 Pedley, H. M. (1990). Syndepositional tectonics affecting Cenozoic and Mesozoic deposition in the Malta and SE  
23 Sicily areas (Central Mediterranean) and their bearing on Mesozoic reservoir development in the N Malta offshore  
24 region. *Marine and Petroleum Geology*, 7(2), 171-180.
- 25 PESA (2008). Petroleum exploration potential of
- 26 Pilcher, R., & Argent, J. (2007). Mega-pockmarks and linear pockmark trains on the West African continental  
27 margin. *Marine Geology*, 244(1-4), 15-32.
- 28 Rebesco, M., & Camerlenghi, A. (Eds.). (2008). *Contourites*. Elsevier.
- 29 Rebesco, M., Hernández-Molina, F. J., Van Rooij, D., & Wählín, A. (2014). Contourites and associated sediments  
30 controlled by deep-water circulation processes: State-of-the-art and future considerations. *Marine Geology*, 352,  
31 111-154.

- 1 Riboulot, Vincent, Antonio Cattaneo, Nabil Sultan, Sebastien Garziglia, Stephan Ker, Patrice Imbert, and Michel  
2 Voisset. "Sea-level change and free gas occurrence influencing a submarine landslide and pockmark formation  
3 and distribution in deepwater Nigeria." *Earth and Planetary Science Letters* 375 (2013): 78-91.
- 4 Roelofse, Chantelle, Tiago M. Alves, and Joana Gafeira. "Structural controls on shallow fluid flow and associated  
5 pockmark fields in the East Breaks area, northern Gulf of Mexico." *Marine and Petroleum Geology* 112 (2020):  
6 104074.
- 7 Sallomo, J. (2012). Seismic Stratigraphy of the Deep Water Area in the Northern Orange Basin Offshore South  
8 Africa. *Search and Discovery Article*, 10389.
- 9 Sayago-Gil, M., Long, D., Hitchen, K., Díaz-del-Río, V., Fernández-Salas, L. M., & Durán-Muñoz, P. (2010).  
10 Evidence for current-controlled morphology along the western slope of Hatton Bank (Rockall Plateau, NE Atlantic  
11 Ocean). *Geo-Marine Letters*, 30(2), 99-111.
- 12 Scarselli, N., McClay, K., & Elders, C. (2016). Seismic geomorphology of Cretaceous megaslides offshore  
13 Namibia (Orange Basin): insights into segmentation and degradation of gravity-driven linked systems. *Marine  
14 and Petroleum Geology*, 75, 151-180.
- 15 Schattner, U., Lazar, M., Souza, L. A. P., Ten Brink, U., & Mahiques, M. M. (2016). Pockmark asymmetry and  
16 seafloor currents in the Santos Basin offshore Brazil. *Geo-Marine Letters*, 36(6), 457-464.
- 17 Shannon, L. V. (1985). The Benguela ecosystem. I: Evolution of the Benguela physical features and processes.  
18 *Oceanography and Marine Biology*, 23, 105-182.
- 19 Sharp, A. and Badalini, G., (2013). Using 3D seismic data to map shallow-marine geohazards: a case study from  
20 the Santos Basin, Brazil. *Petroleum Geoscience*, 19(2), pp.157-167.
- 21 Sharp, A., & Samuel, A. (2004). An example study using conventional 3D seismic data to delineate shallow gas  
22 drilling hazards from the West Delta Deep Marine Concession, offshore Nile Delta, Egypt. *Petroleum Geoscience*,  
23 10(2), 121-129.
- 24 Stow, D. A. V., Hunter, S., Wilkinson, D., & Hernández-Molina, F. J. (2008). The nature of contourite deposition.  
25 *Developments in sedimentology*, 60, 143-156.
- 26 Sun, Q., Wu, S., Hovland, M., Luo, P., Lu, Y., & Qu, T. (2011). The morphologies and genesis of mega-pockmarks  
27 near the Xisha Uplift, South China Sea. *Marine and Petroleum Geology*, 28(6), 1146-1156.
- 28 the orange basin. Available online at [https://www.petroileumagencysa.com/images/pdfs/Orange\\_Basin\\_Brochure-  
JS-02-18w1.pdf](https://www.petroileumagencysa.com/images/pdfs/Orange_Basin_Brochure-<br/>29 JS-02-18w1.pdf)
- 30 Uenzelmann-Neben, G., & Huhn, K. (2009). Sedimentary deposits on the southern South African continental  
31 margin: Slumping versus non-deposition or erosion by oceanic currents?. *Marine Geology*, 266(1-4), 65-79.

1 Uenzelmann-Neben, G., Schlüter, P., & Weigelt, E. (2007). Cenozoic oceanic circulation within the South African  
2 gateway: indications from seismic stratigraphy. *South African Journal of Geology*, 110(2-3), 275-294.

3 Van der Spuy, D. (2003). Aptian source rocks in some South African Cretaceous basins. *Geological Society,  
4 London, Special Publications*, 207(1), 185-202.

5 Viola, G., Andreoli, M., Ben-Avraham, Z., Stengel, I., & Reshef, M. (2005). Offshore mud volcanoes and onland  
6 faulting in southwestern Africa: neotectonic implications and constraints on the regional stress field. *Earth and  
7 Planetary Science Letters*, 231(1-2), 147-160.

8 Wefer, G., Berger, W.H., Richter, C., et al., (1998). Proceedings of the Ocean Drilling Program, Initial Reports,  
9 Vol. 175

10 Weigelt, E., & Uenzelmann-Neben, G. (2004). Sediment deposits in the Cape Basin: Indications for shifting ocean  
11 currents? AAPG bulletin, 88(6), 765-780.

12 Wenau, S., Spiess, V., & Zabel, M. (2021). Giant seafloor depressions caused by slope failures and bottom  
13 currents on the Namibia continental margin. *Geochemistry, Geophysics, Geosystems*, 22(7), e2020GC009548.

14  
15  
16  
17  
18  
19  
20  
21  
22  
23  
24  
25  
26  
27  
28  
29  
30  
31  
32  
33  
34

## 1 List of Figures

2 **Figure 1.** Location of the study area. (a) Location map of the Orange Basin and the study area along the  
3 southwestern African continental margin. The map also includes the datasets used in this study and the active  
4 marine source rock kitchen at the lower Aptian level (Jungslager 1999). The topography and bathymetry map are  
5 adopted from the Gridded Bathymetry Chart of the Oceans (GEBCO). The BC (Benguela Current) and BOC  
6 (Benguela Coastal Current BCC) are surface currents, while the AAIW (Antarctic Intermediate Water), NADW  
7 (North Atlantic Deepwater), and AABW (Antarctic Bottom water) are deeper water masses (Uenzelmann-Neben  
8 et al. 2007).

9  
10 **Figure 2.** Configuration of the Orange Basin and chrono lithostratigraphy. (a) Generalized stratigraphic cross  
11 section of the Orange Basin modified from (Jungslager 1999; Sallomo 2012). Location of the cross-section is  
12 shown in Figure 1. Location of the ODP 1087 borehole and extent of the study area projected. (b)  
13 Chronostratigraphic and sequence stratigraphic chart for the Orange Basin including the tectonic phases and  
14 events (Séranne and Anka 2005; Scarselli et al. 2016). (c) Gamma ray log and lithology of the ODP Leg 175  
15 borehole 1087a (Wefer et al., 1998). Location of ODP borehole 1087a is shown in Figure 1).

16  
17 **Figure 3.** (a) Close up of a typical elongated pockmark (location shown in Figure 5), showing GIS delineated  
18 pockmark outline and the long and short axes. (b) An illustration of the pockmark extraction process, whereby the  
19 water depth is defined as the depth to the smoothed seafloor, and the pockmark depth is defined as the distance  
20 between the deepest point within the pockmark to the smoothed seafloor atop of it. Diagram modified from Gaferia  
21 et al. (2012).

22  
23 **Figure 4.** Along the slope seismic profile showing (a) uninterpreted and (b) the interpreted seismic stratigraphy  
24 of the slope. Location of seismic profile is shown in Figure 1.

25  
26 **Figure 5.** Seafloor geomorphology (a) Uninterpreted bathymetric map derived from the 3D seismic data (b)  
27 Variance map extracted along the seafloor showing a better delineation of edges and depression along the seafloor.  
28 Interpretation of both maps is presented in Figure 4. Location of map is shown in Figure 1.

29  
30 **Figure 6.** Various end-members of pockmarks mapped on the seafloor. (a) Crescentic pockmarks, circular  
31 pockmarks, and a linear array of circular pockmarks (b) Circular pockmarks (c) Comet-shaped pockmarks,  
32 irregular depressions, elongated pockmark and channel-like morphologies. Location of figures is shown in Figure  
33 5c.

34  
35 **Figure 7.** Classification of the seafloor into zones with interpreted geomorphologies: pockmarks, irregular  
36 depressions and channel-like morphologies from Figures 5 and 6. Rose diagrams show the orientation of  
37 depression in each zone. AAIW = Antarctic Intermediate Water current and NADW = North Atlantic Deepwater  
38 current.

39  
40

1 **Figure 8. (a -b)** Composite seismic profiles showing the seafloor pockmarks in Zone 2a. MTC= Mass transport  
2 complex. Location of profile is shown in Figure 5a.  
3

4 **Figure 9 (a-b)** Composite seismic profile showing that the seafloor pockmarks developed above the buried  
5 turbidite channel system (in 9a for Zone1 and 9b for zone 2). Some channels are close to shallow faults which  
6 may promote localized fluid flow. MTC= Mass transport complex. Location of profile is shown in Figure 5a.  
7

8 **Figure 10. (a)** Composite seismic profile showing the seafloor pockmarks developing above buried turbidite  
9 channels. Notice the presence of localized amplitude anomalies in the Cenozoic succession which may represent  
10 sequestered fluids. Faults emanating from the Cretaceous Megaslide Complex may serve as conduit for  
11 transporting biogenic fluids to the overburden. (b) Seismic profile showing pockmarks developed above a buried  
12 channel and erosional flank related to the contourite deposits (c) Seismic profile showing a pockmark developed  
13 above buried MTC. MTC= Mass transport complex. Location of profile is shown in Figure 5a  
14

15 **Figure 11. (a-c)** Composite seismic profile showing pockmarks and irregular depressions on the seafloor. Notice  
16 the shallow gas anomaly in the near seafloor sediments in Figure 11a. MTC= Mass transport complex. Location  
17 of profile is shown in Figure 5a  
18

19 **Figure 12.** Spatial alignment of seafloor pockmarks and other depressions with respect to buried geomorphologic  
20 features. (a) Variance surface slice 100 ms TWT below the seafloor showing the manifestation of buried turbidite  
21 channels, erosional flanks, and buried mass transport deposits (b) Pockmarks and other depressions mapped along  
22 the seafloor showing spatial alignment with the buried turbidite channel morphologies and erosional edges.  
23

24 **Figure 13.** Pockmark morphometric parameters across different zones in the study area. (a) Pockmark depth  
25 versus water depth (b) Pockmark axis length versus water depth. (c) Pockmark area versus pockmark depth (d)  
26 Pockmark axis length versus pockmark depth. (e) Box plot showing the distribution of pockmark depth and  
27 pockmark long axis (diameter) across the seafloor zones. (f) Comparison of pockmark size in this study to those  
28 obtained globally. Graph illustrates the pockmark geometry of previously studied pockmarks from 58 published  
29 sites, compiled by Pilcher and Argent (2007) and modified by Karaket et al. (2021) in comparison with dimension  
30 of pockmarks in this study. The X and Y scales are logarithmic. The paleo-pockmark geometry of this study is  
31 presented by a red. The single points represent either measurements of single pockmarks or average measurements  
32 and the error bars represent the range of sizes in a pockmark field.  
33

34 **Figure 14. (a)** Conceptual model illustrating fluid migration and formation of seafloor pockmarks along the slope  
35 of the Orange Basin. (b) Evolutionary model for the formation of the crescentic and elongated pockmarks in the  
36 study illustrating the post-formation modification of initial pockmark morphology by bottom currents operating  
37 in the study area. See text for more detail.  
38  
39  
40

1  
2  
3  
4  
5  
6  
7  
8  
9  
10  
11  
12  
13  
14  
15  
16  
17  
18

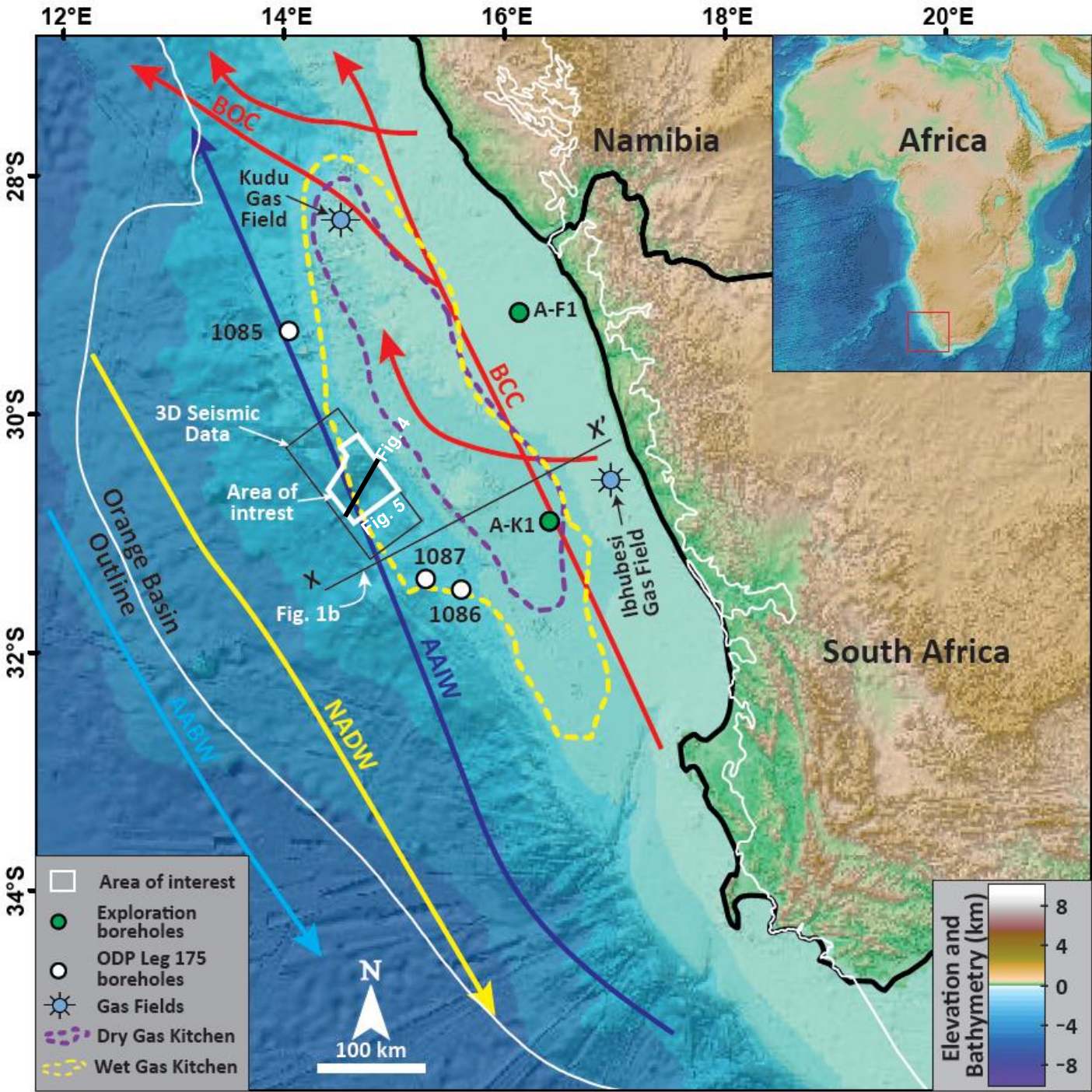


Figure 1

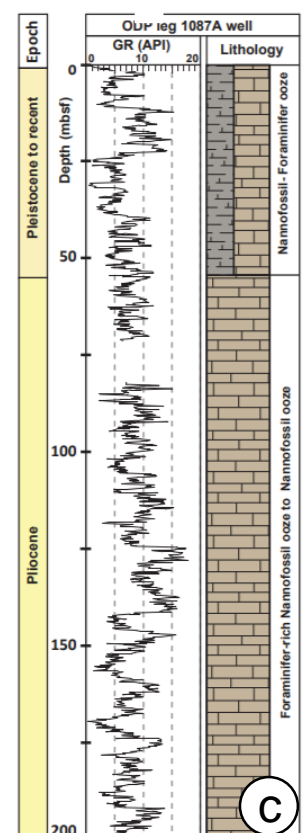
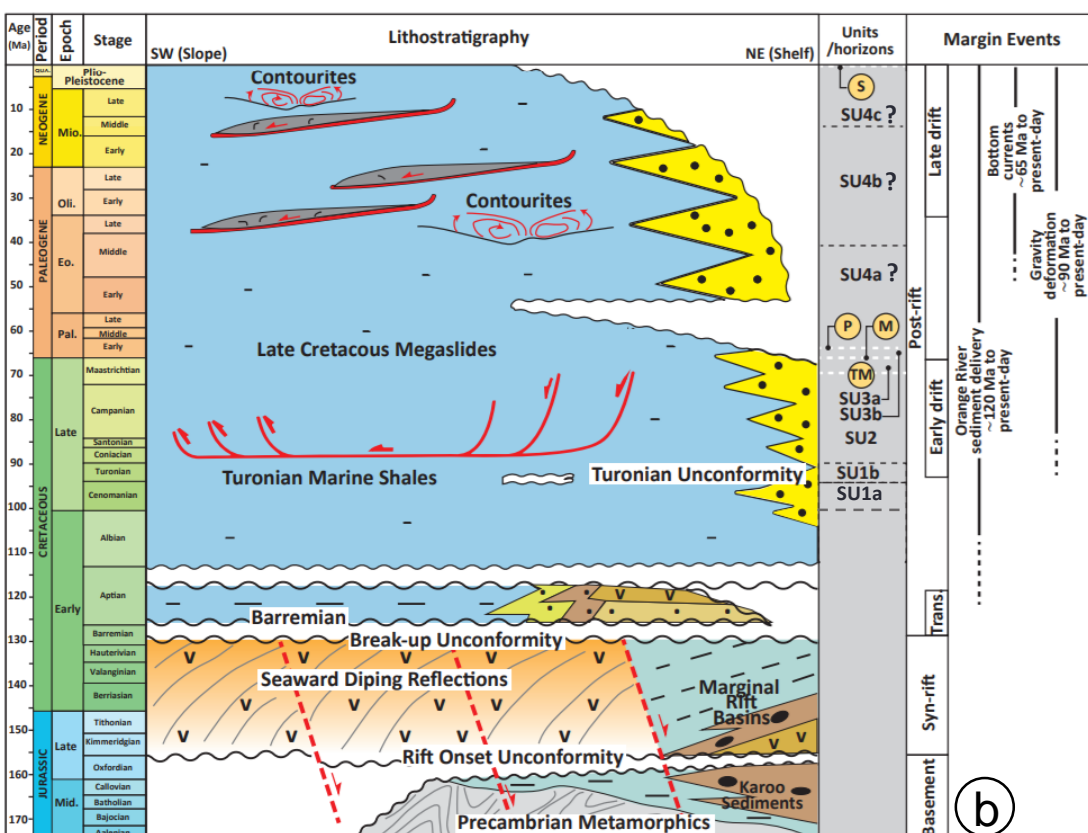
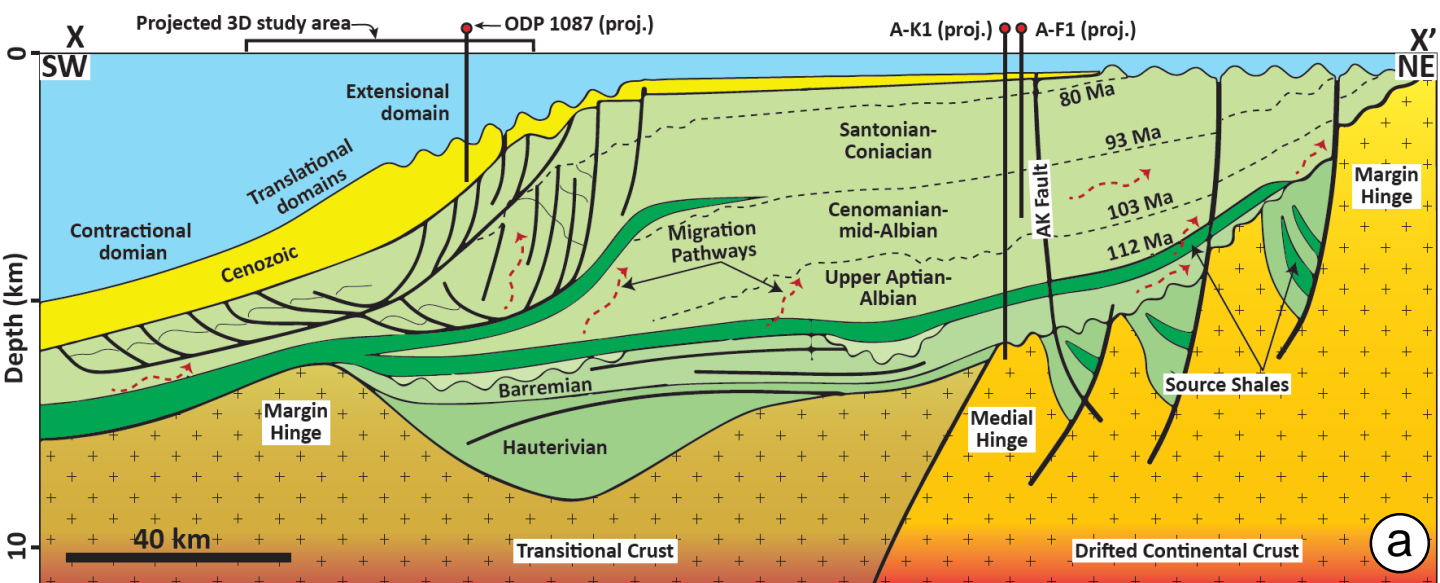


Figure 2

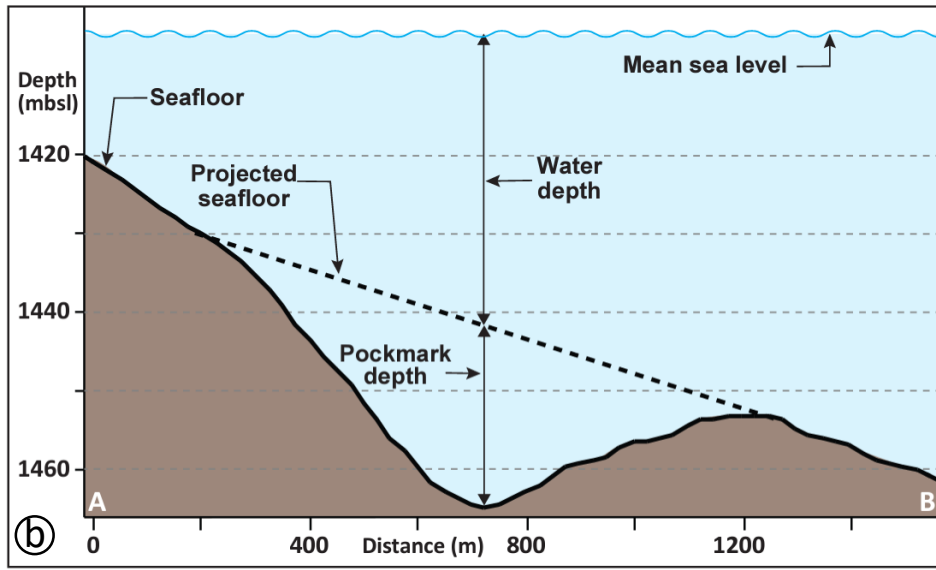
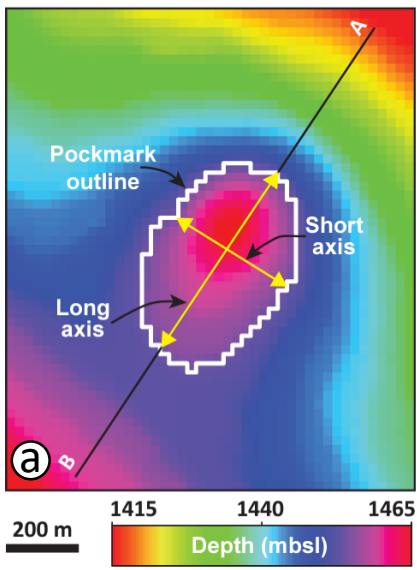


Figure 3

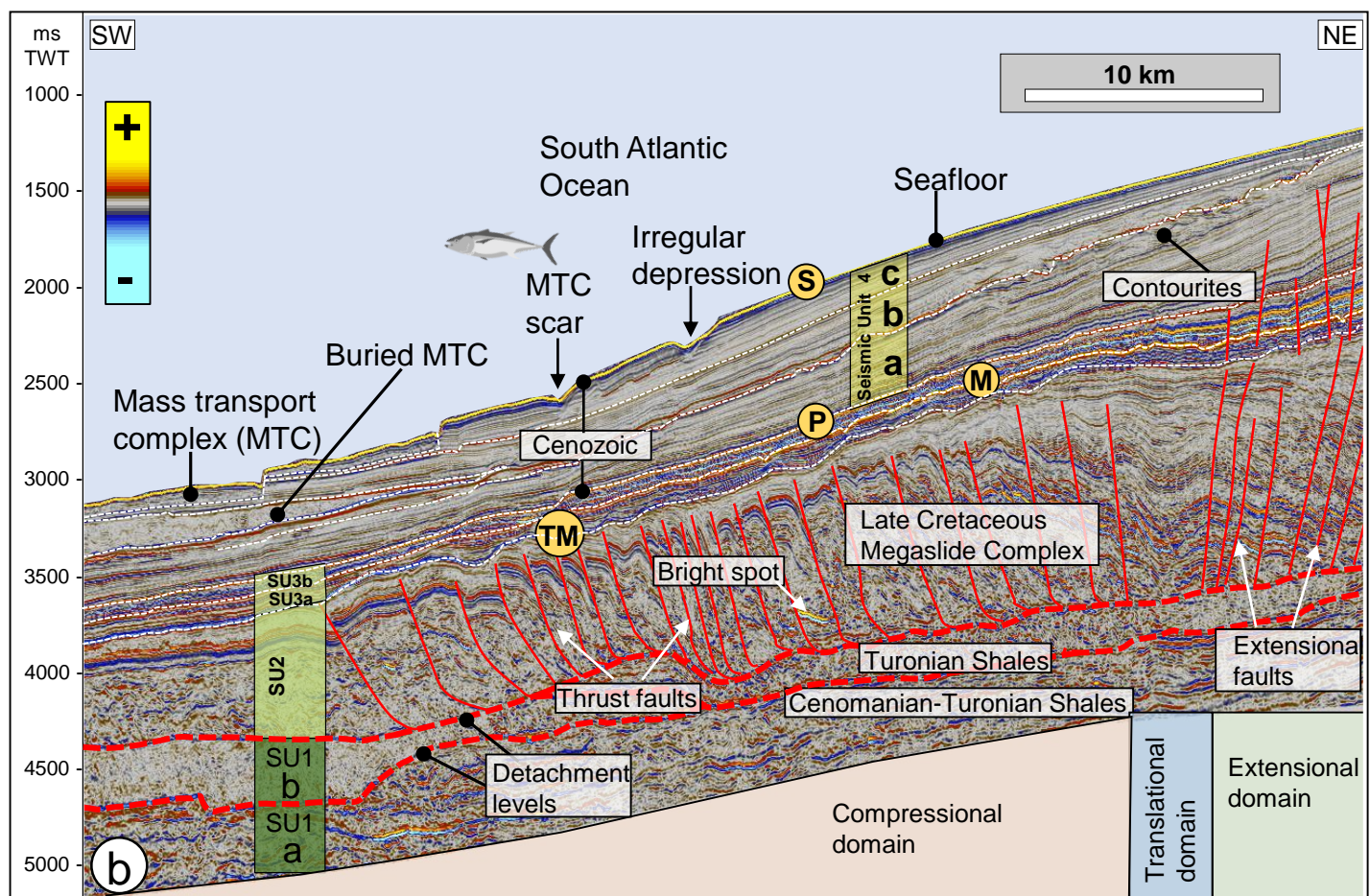
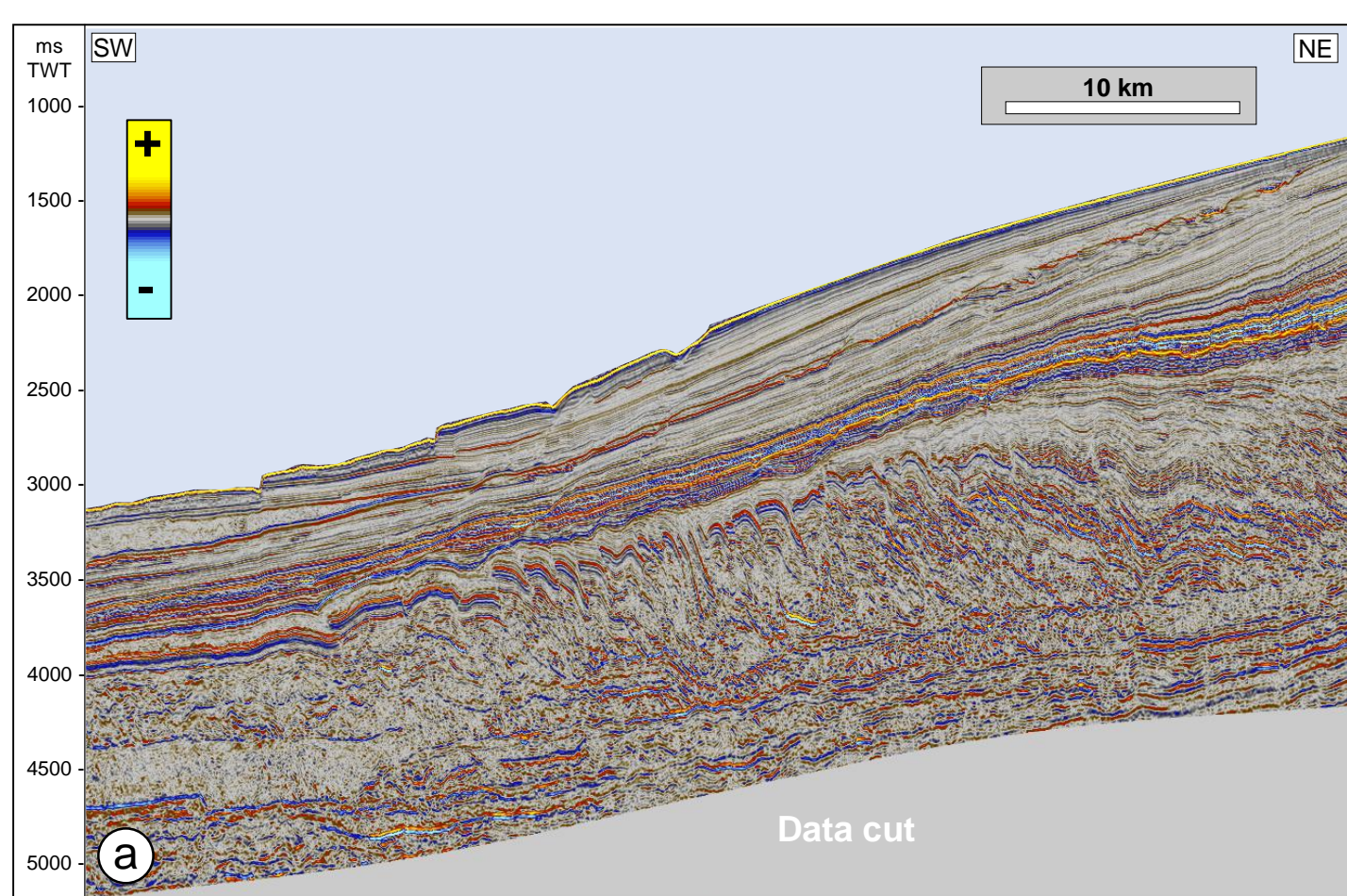


Figure 4

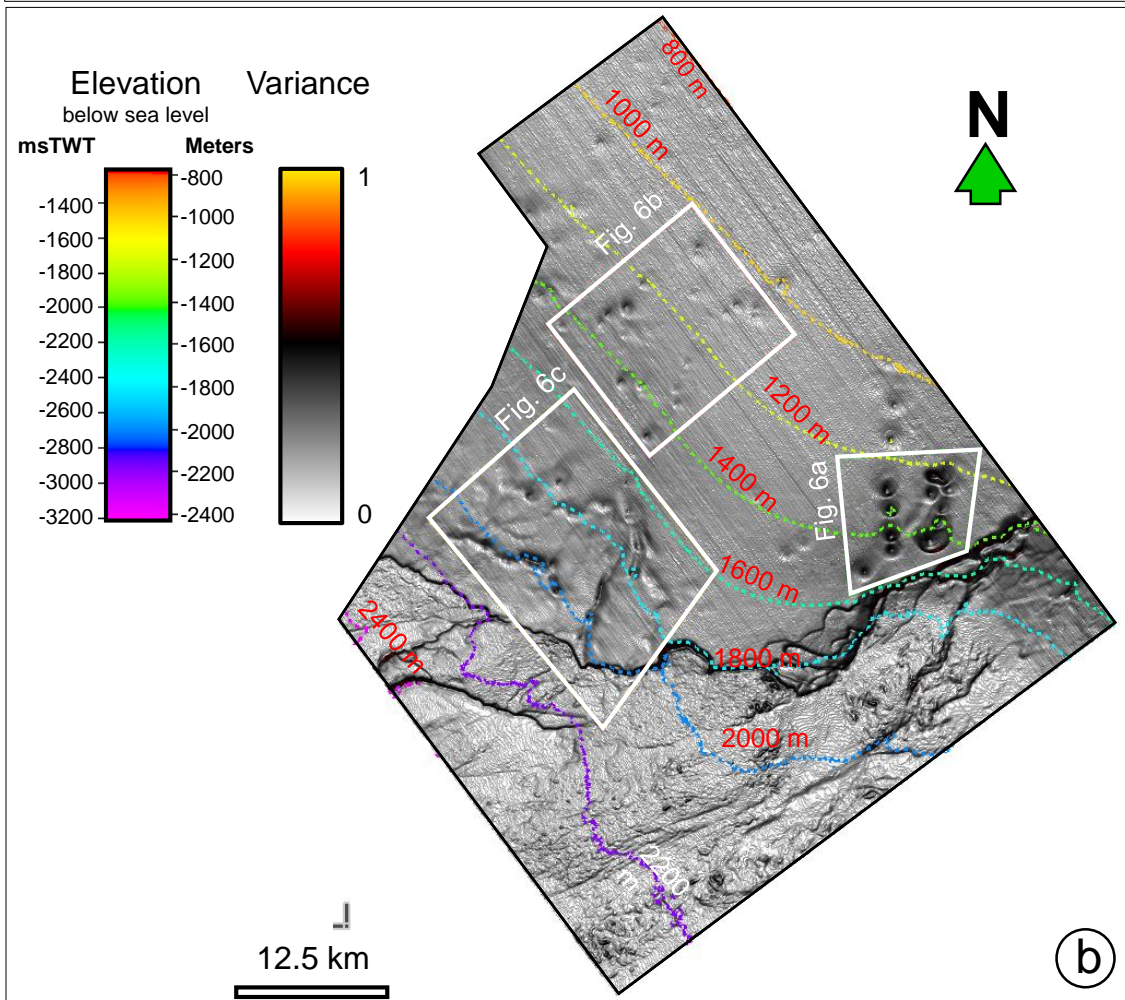
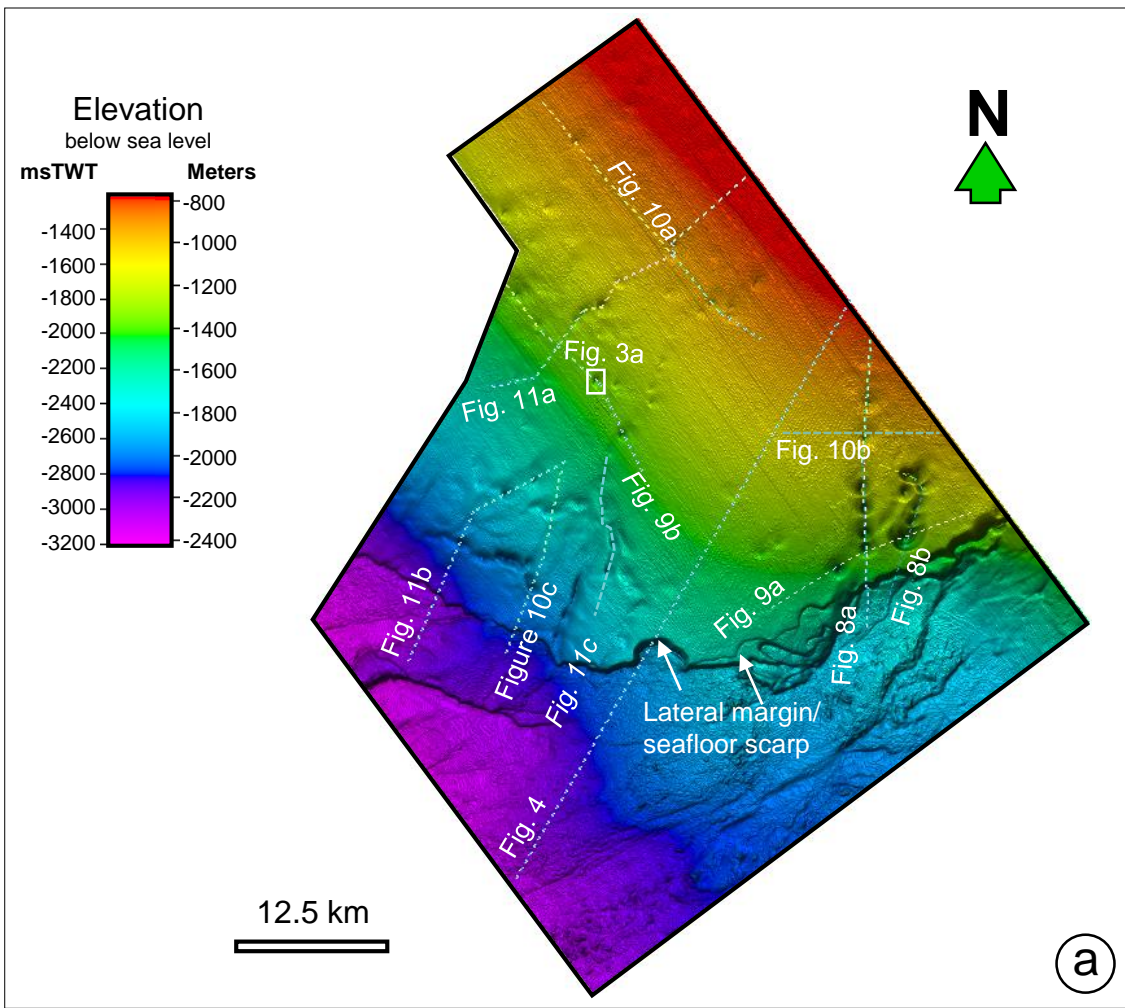


Figure 5

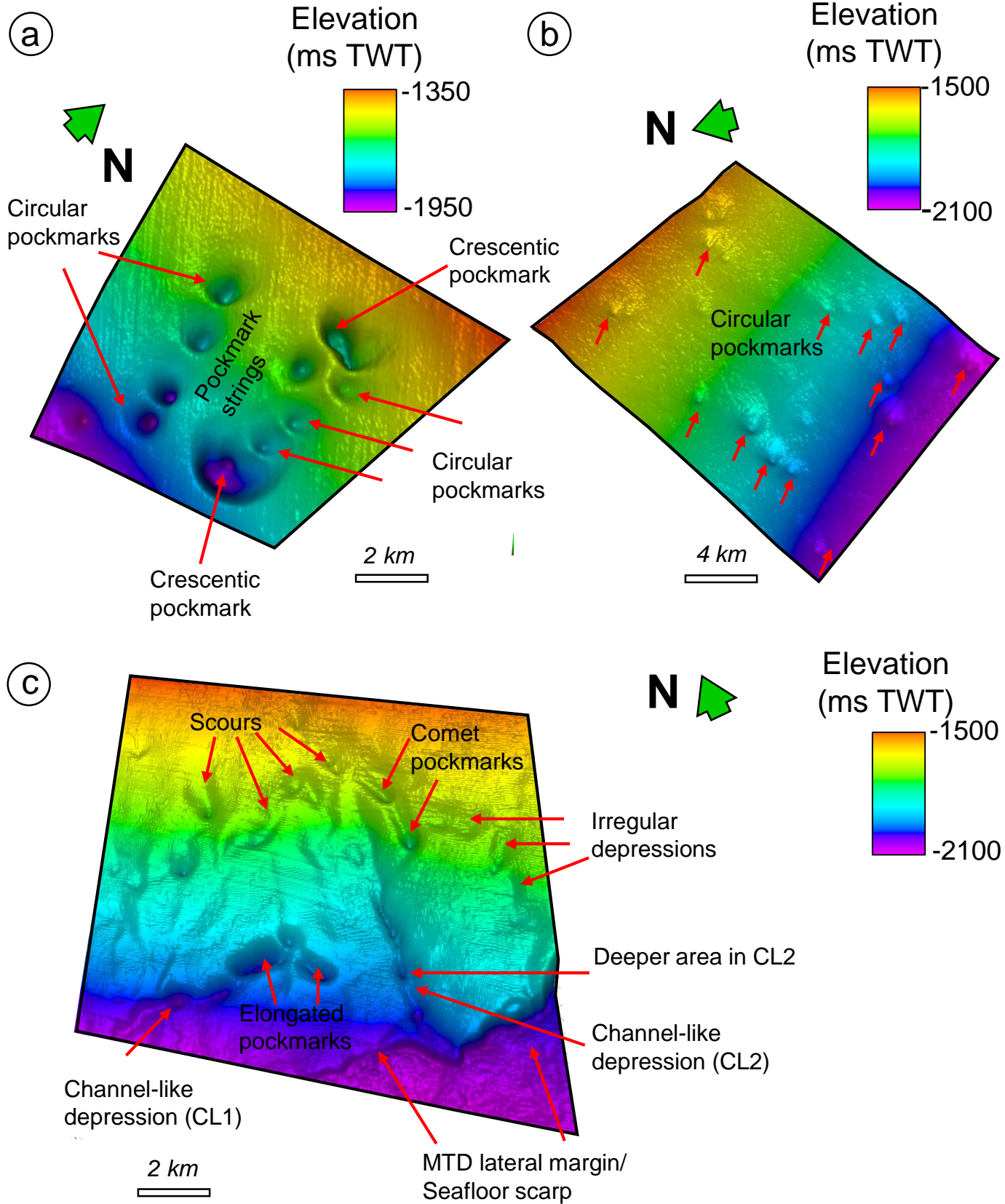


Figure 6

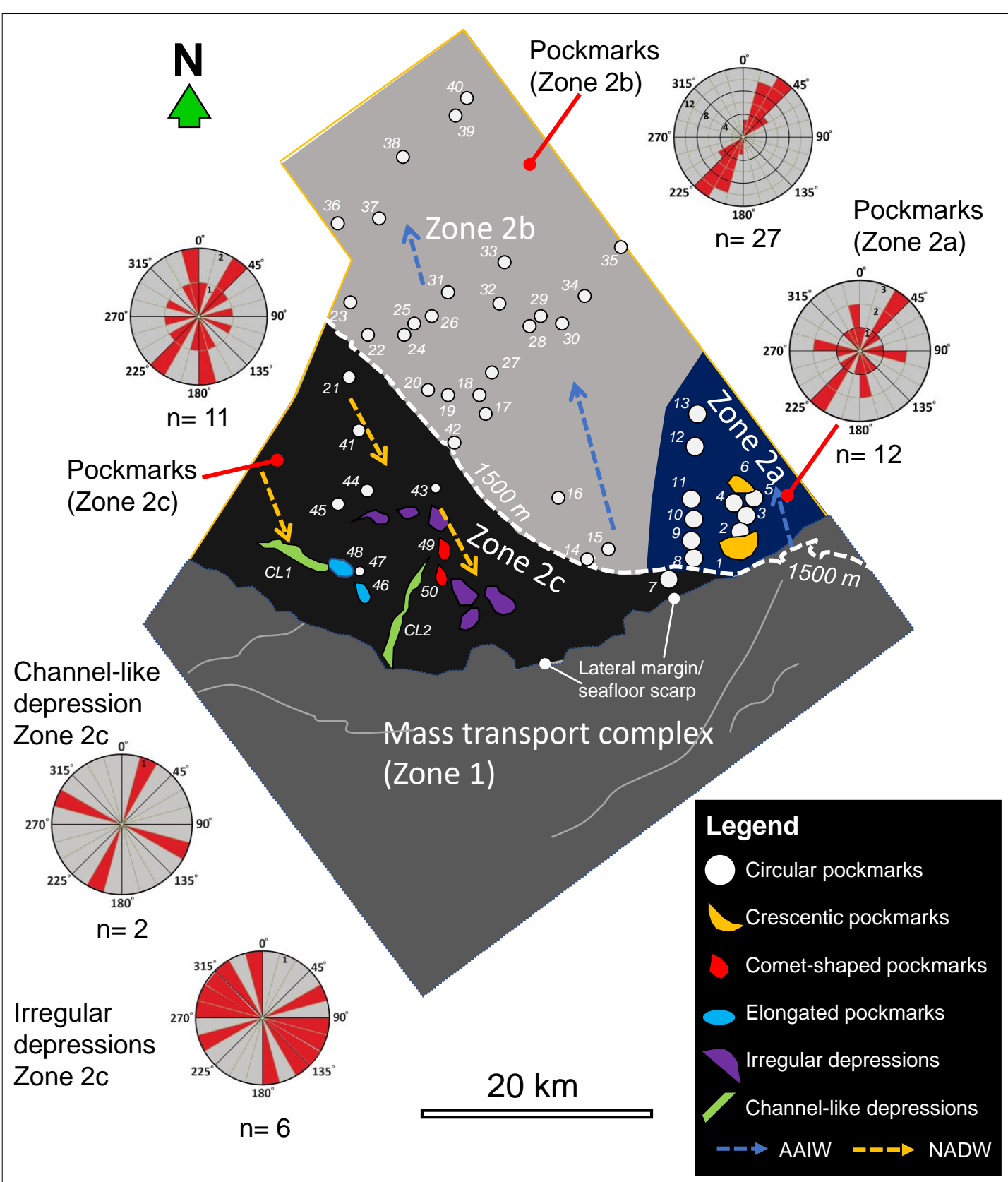


Figure 7

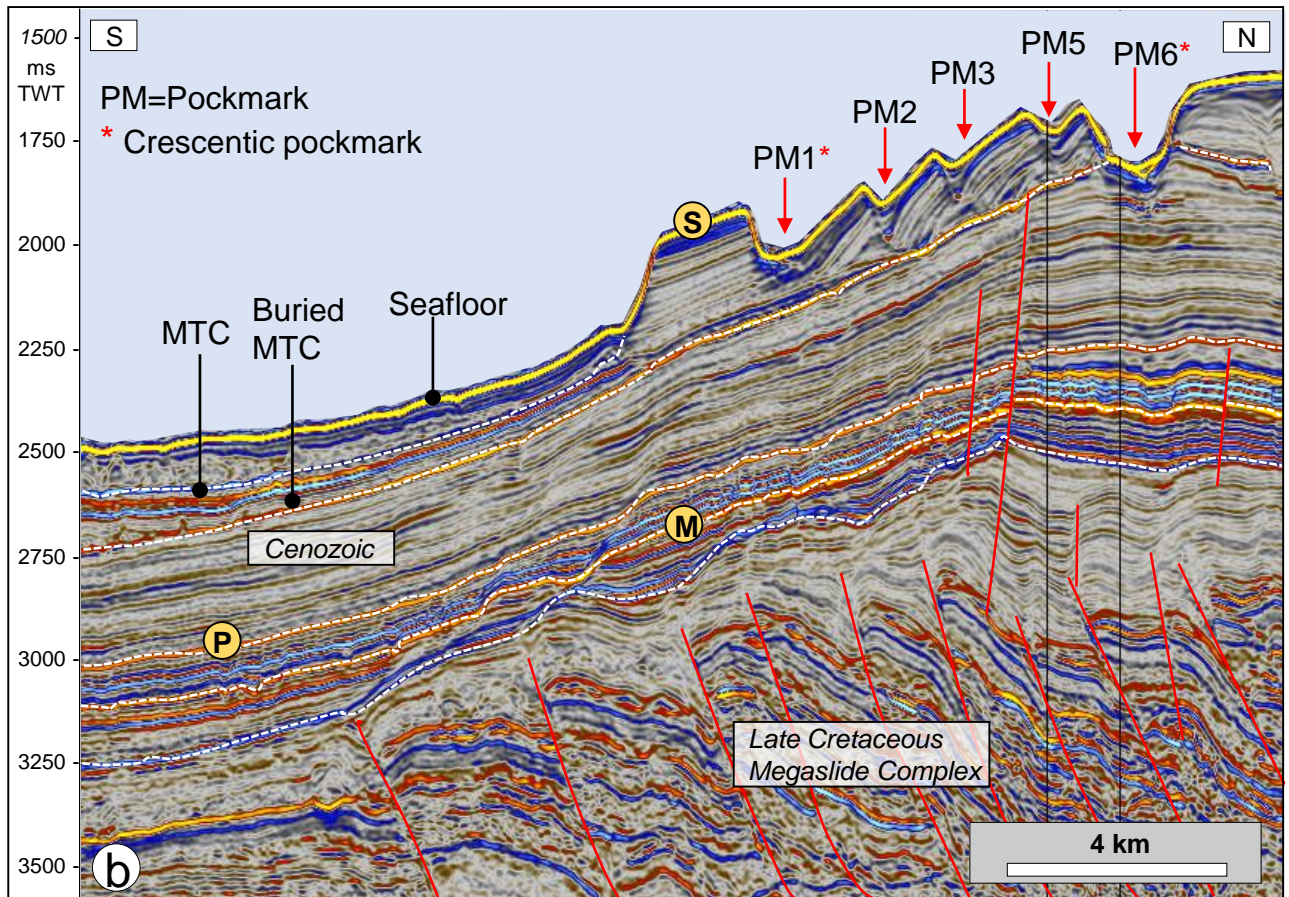
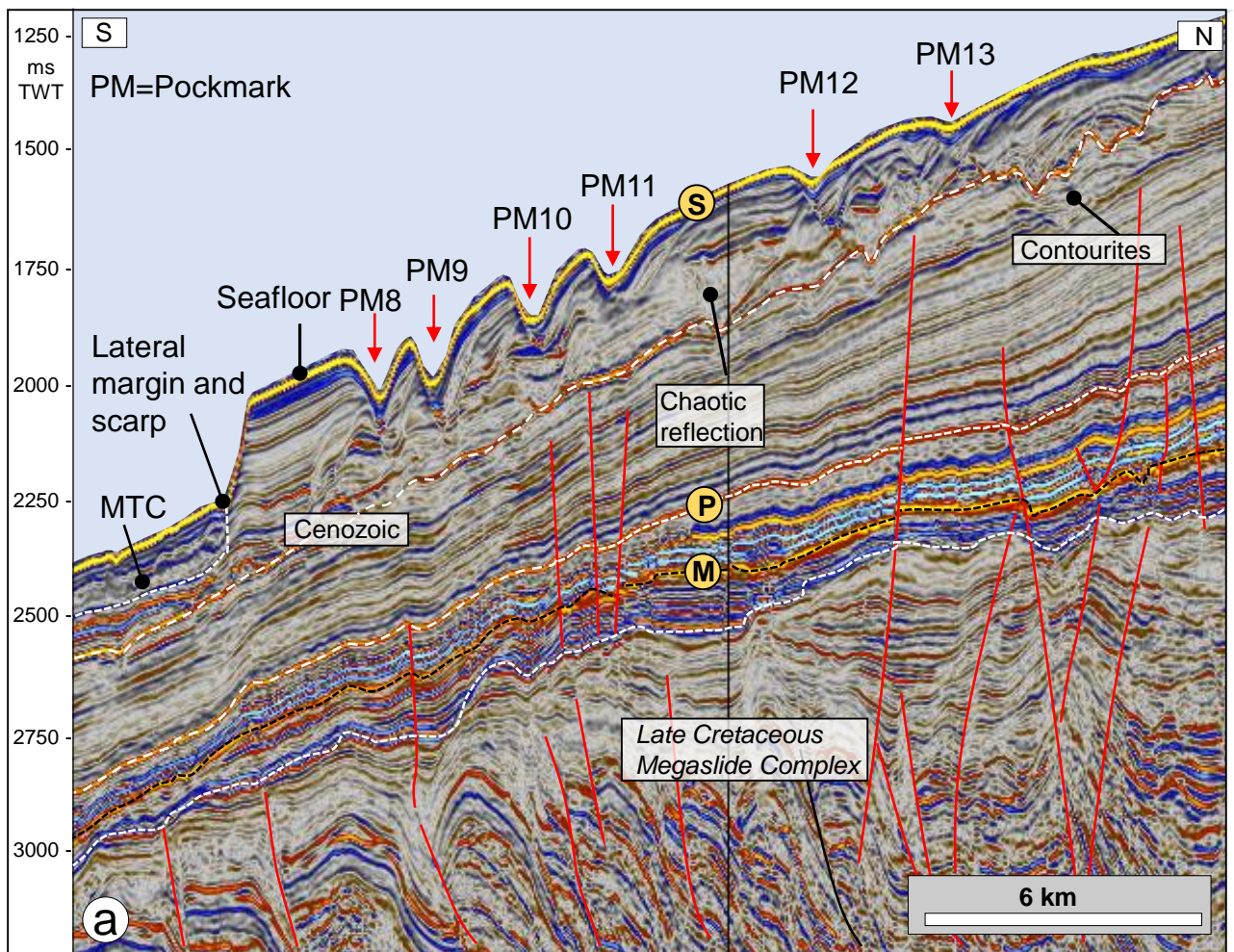


Figure 8

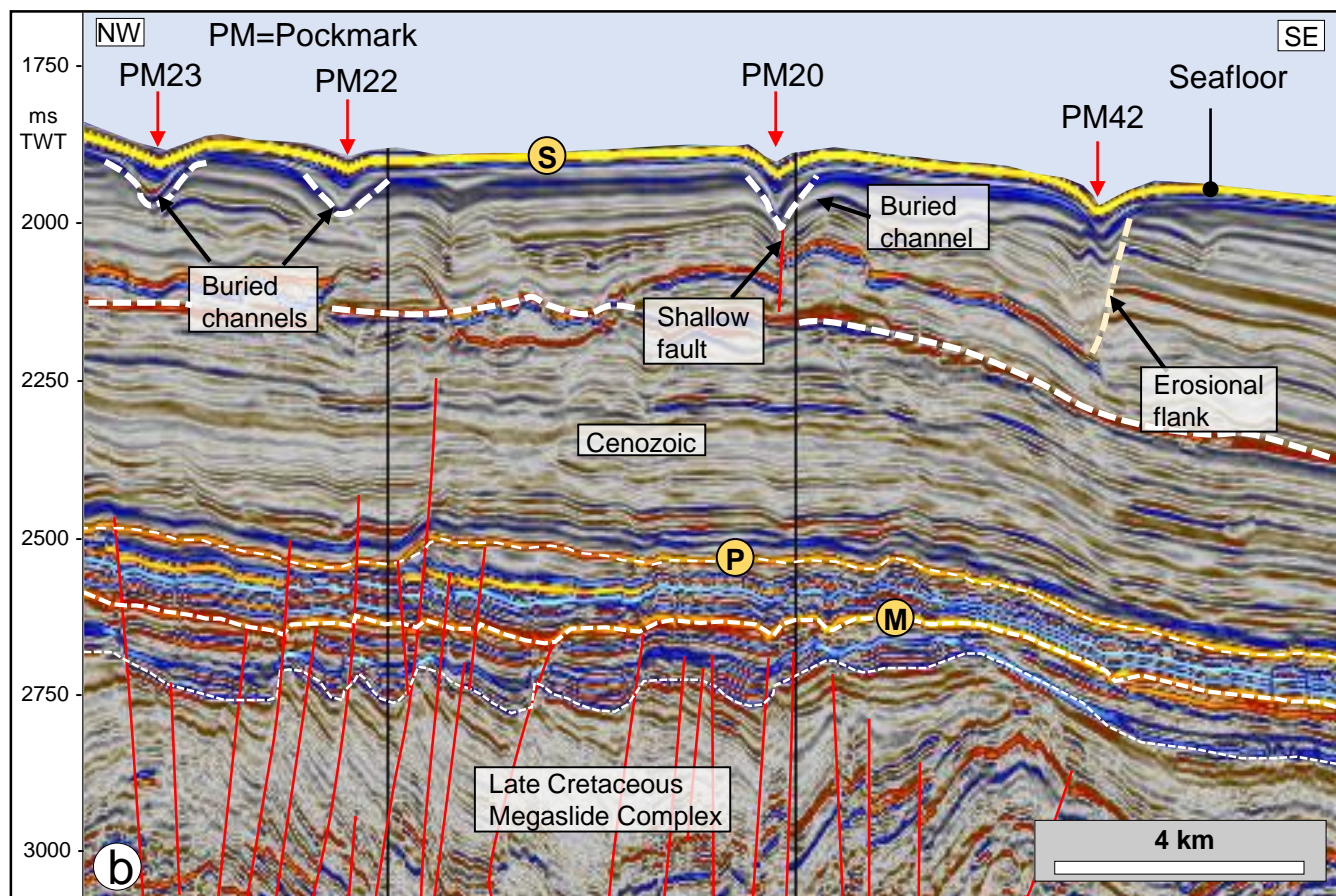
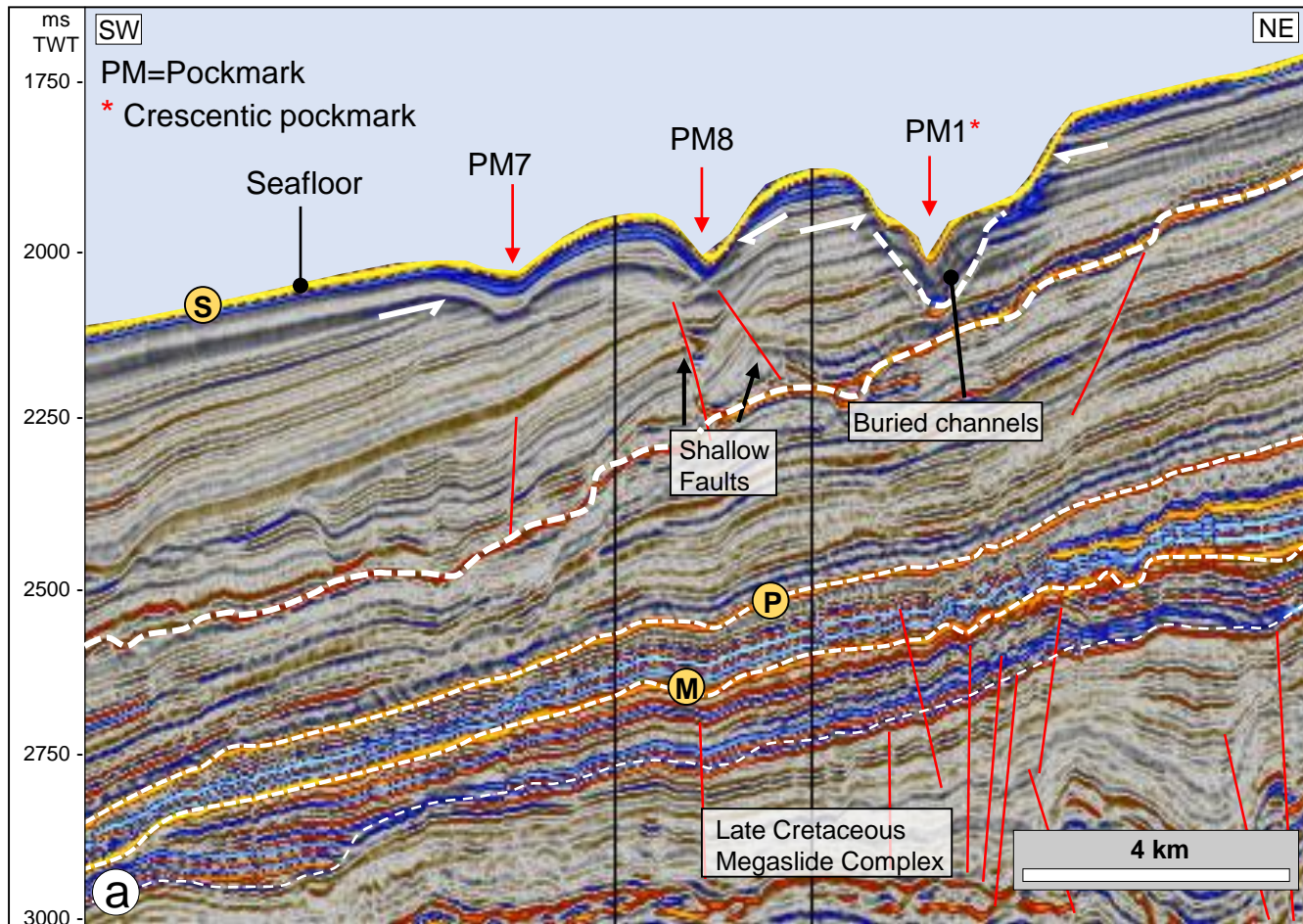


Figure 9

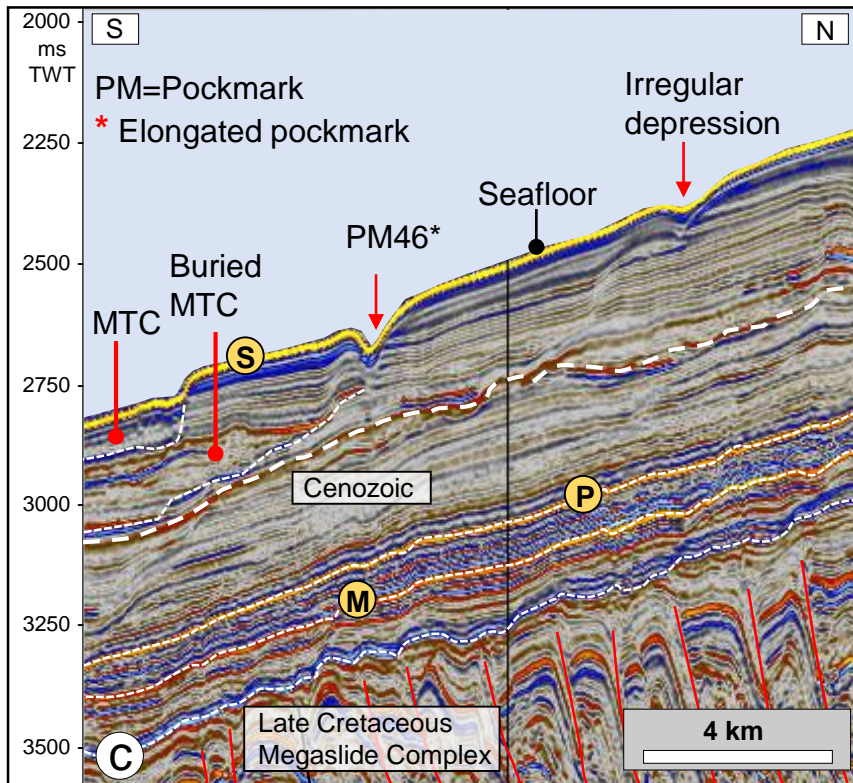
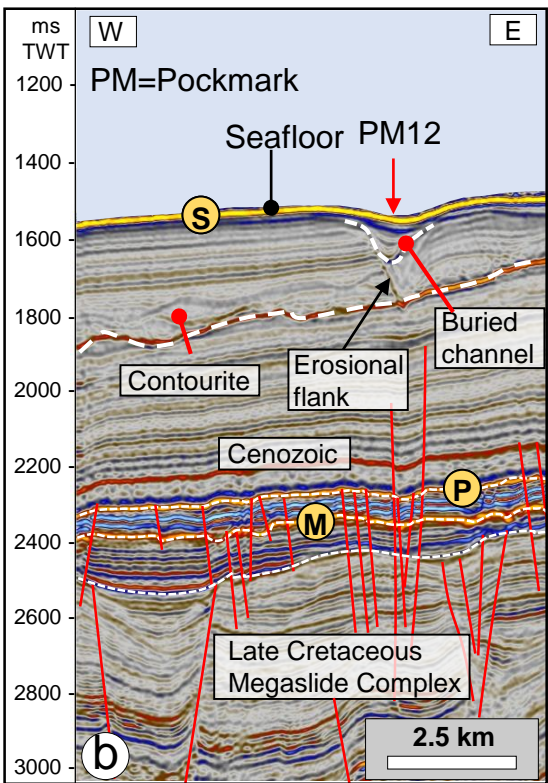
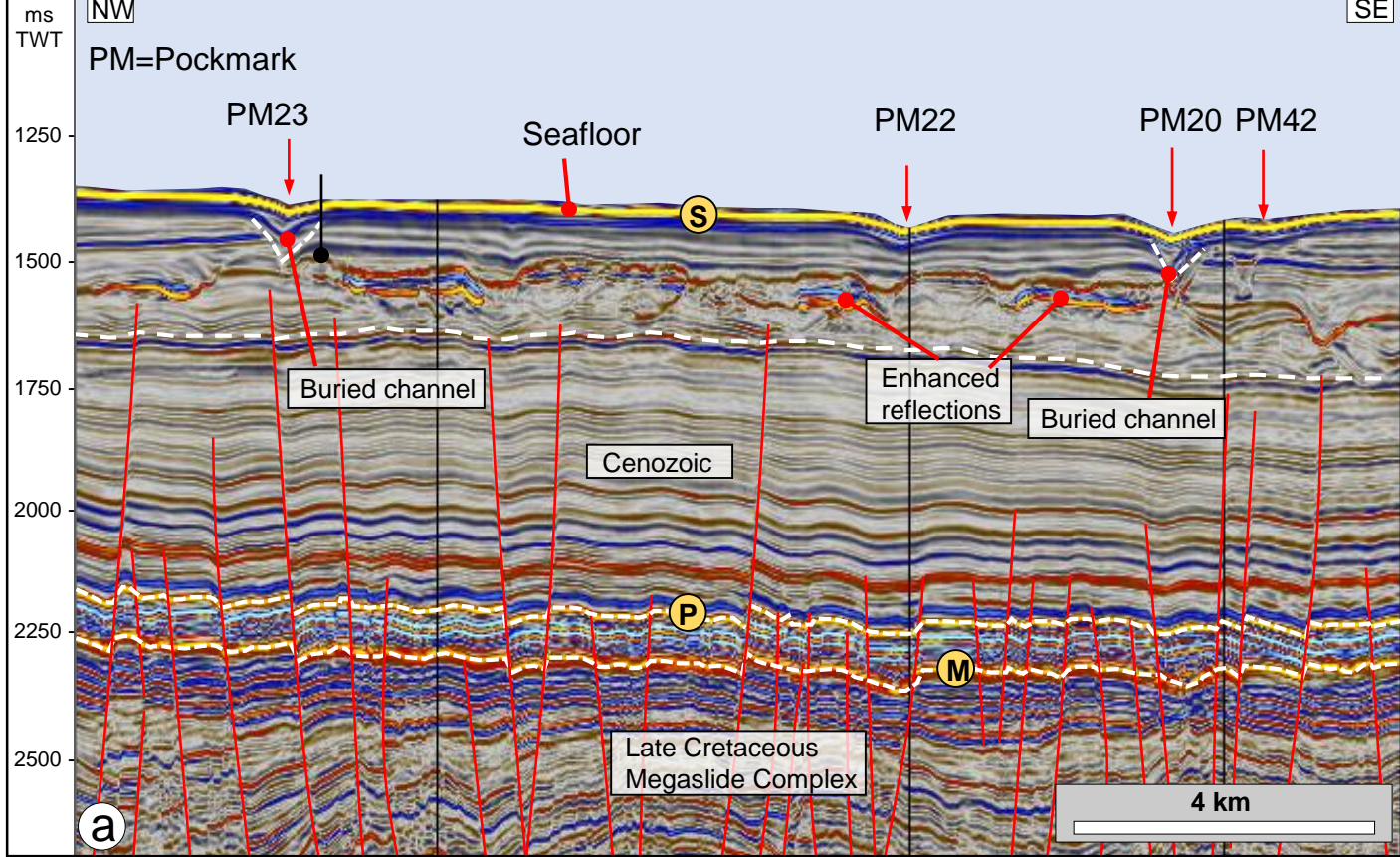


Figure 10

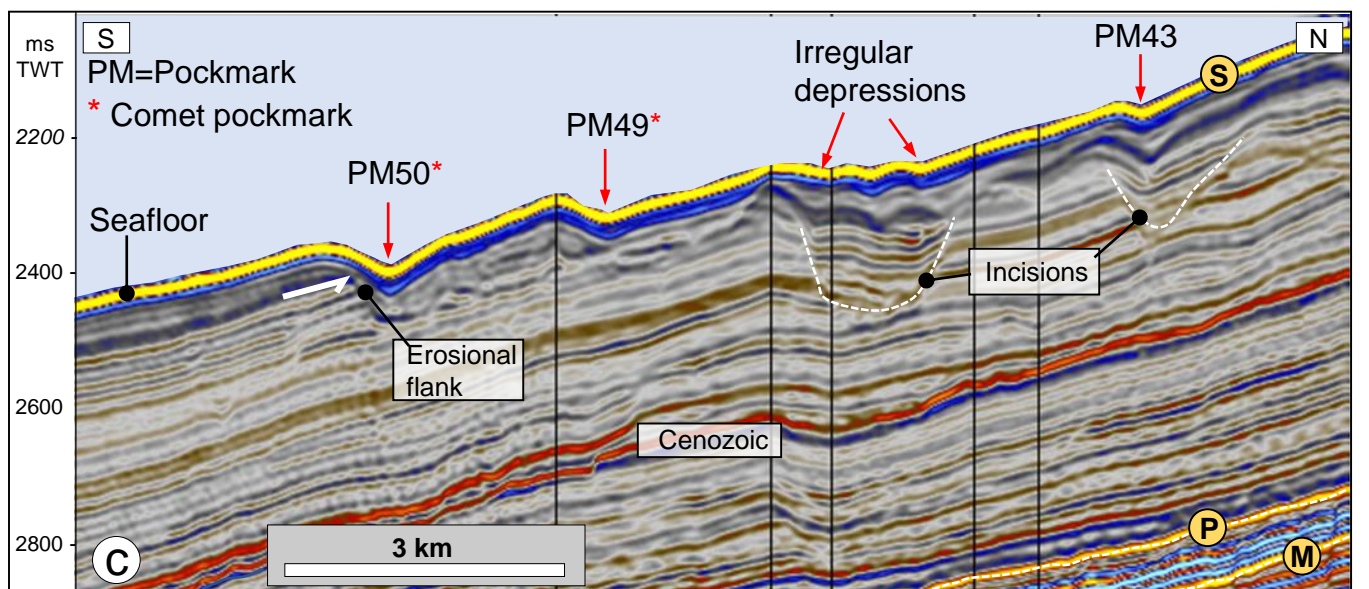
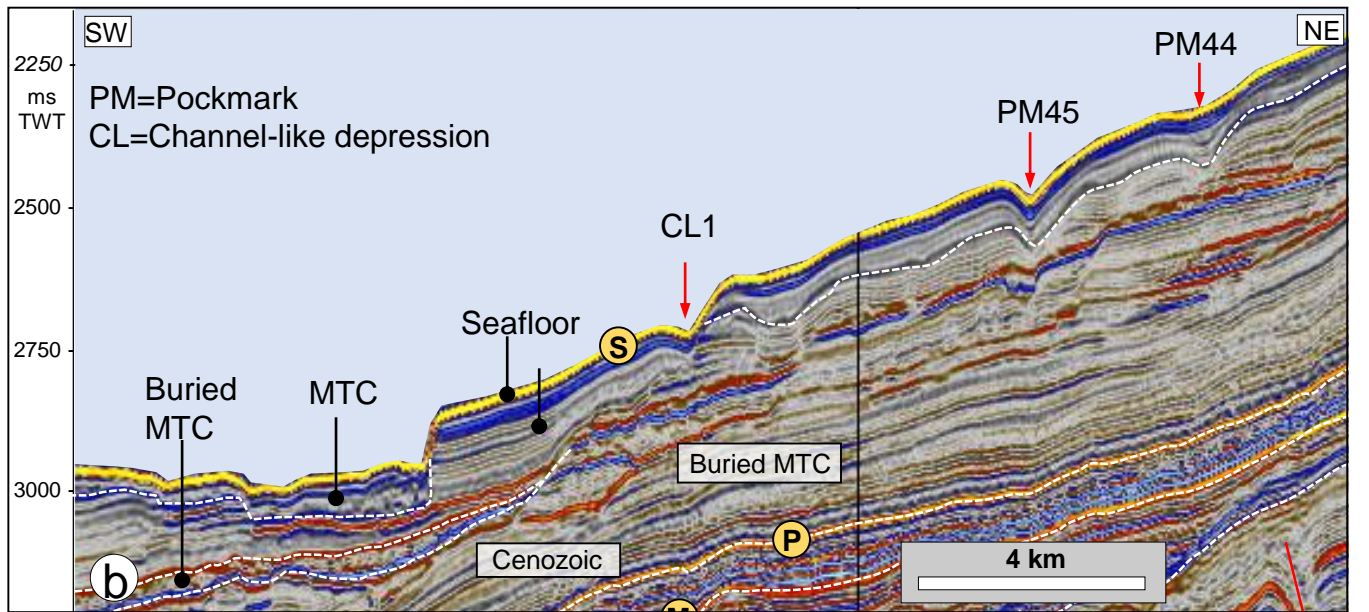
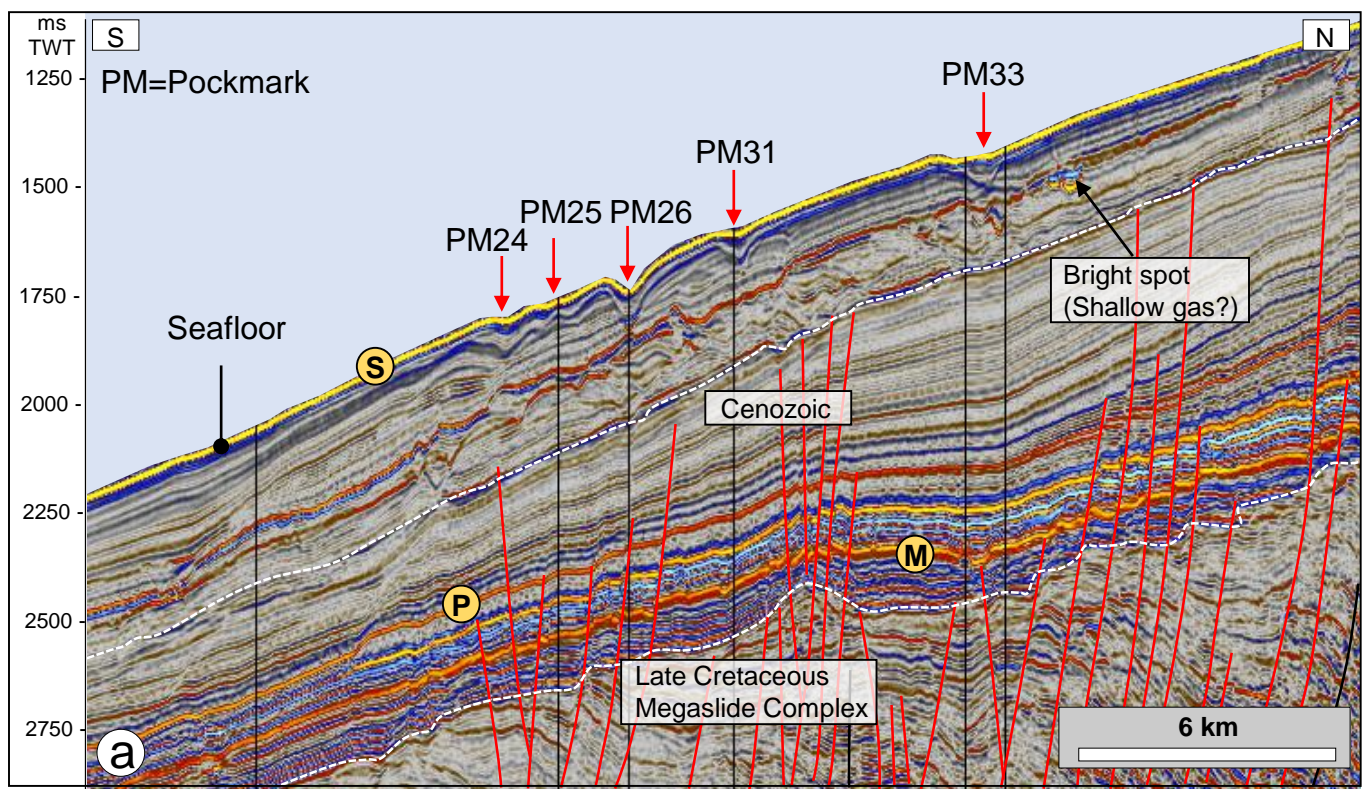


Figure 11

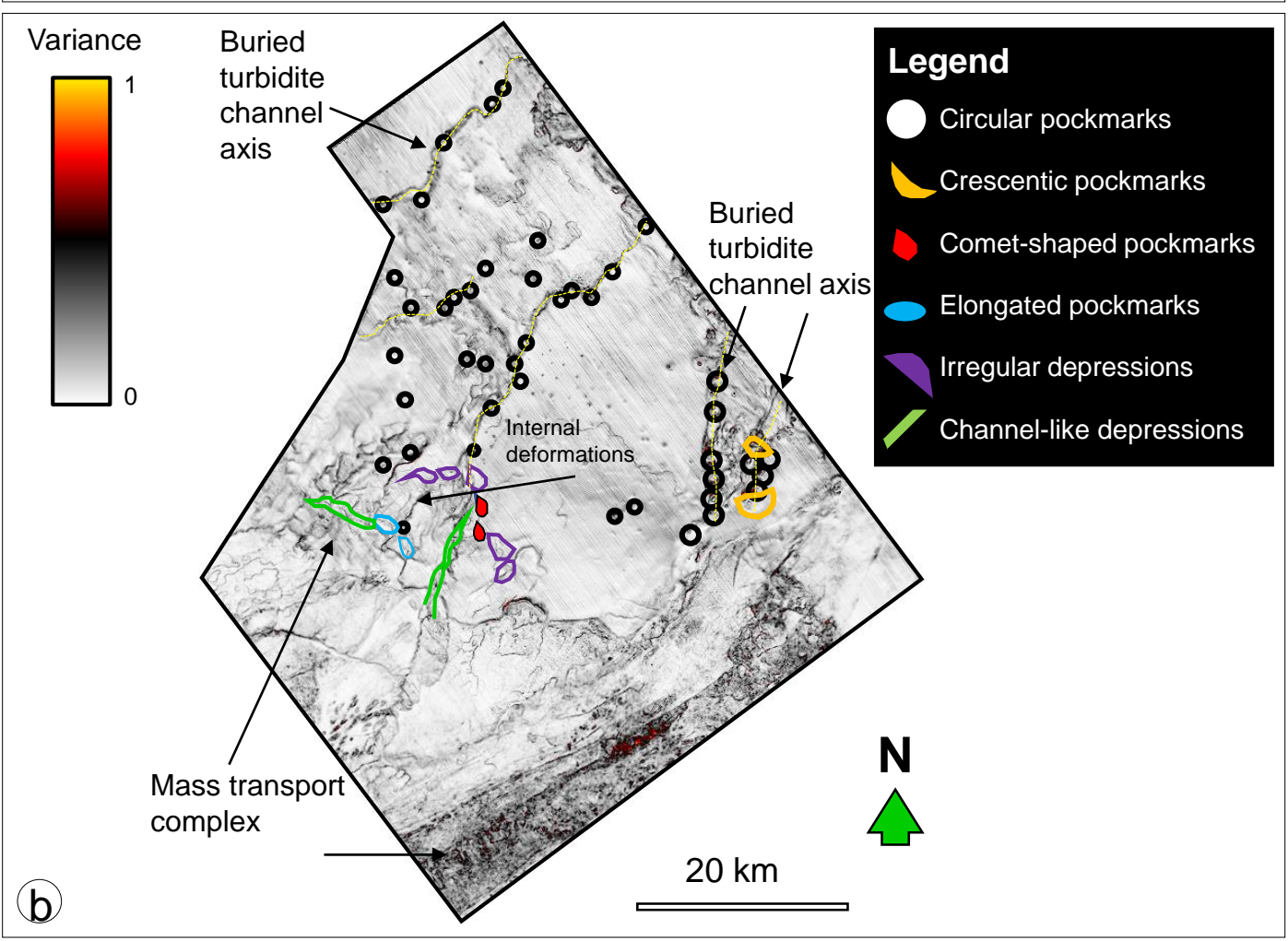
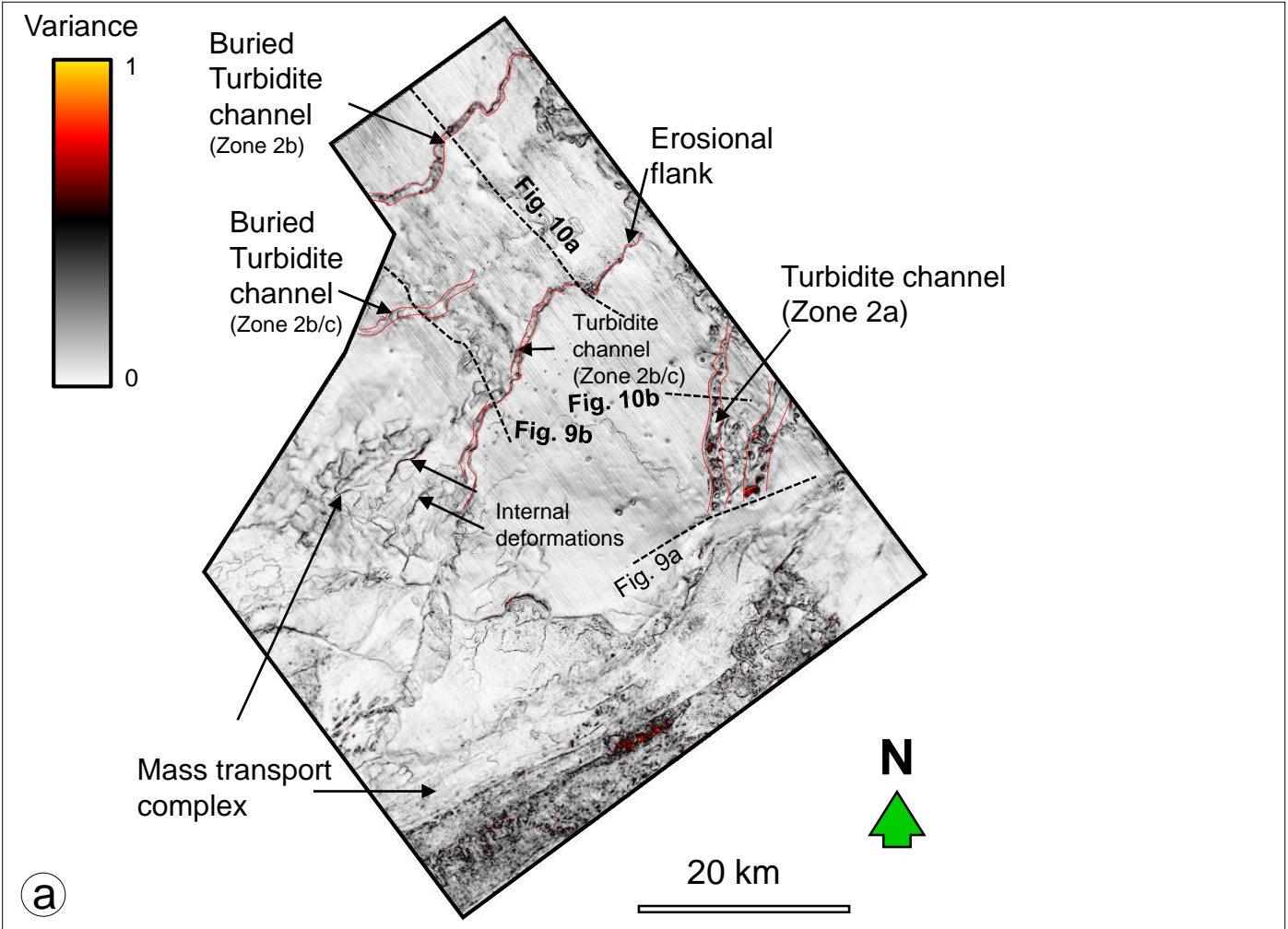
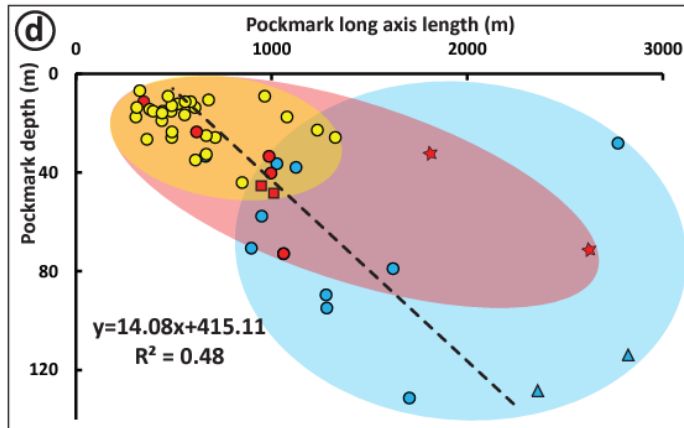
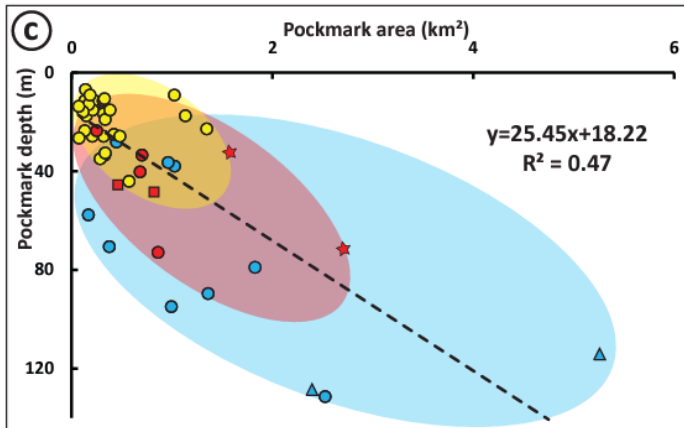
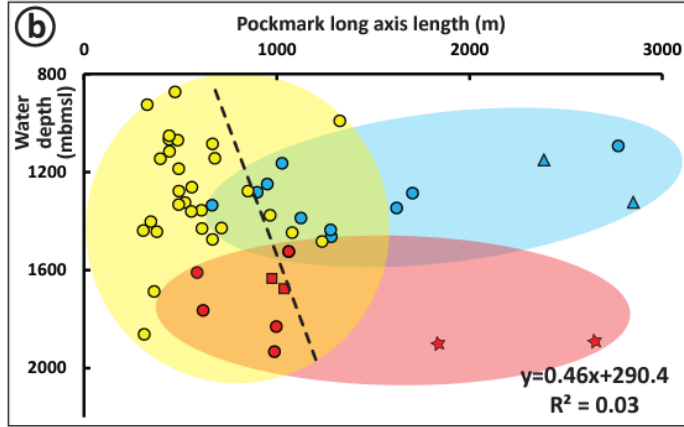
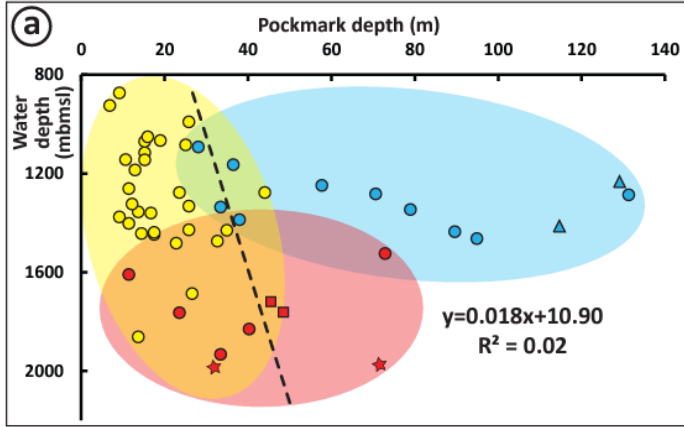


Figure 12



■ Zone 2a    ■ Zone 2b    ■ Zone 2c    ○ Circular    □ Comet    △ Crescentic    ☆ Elongated

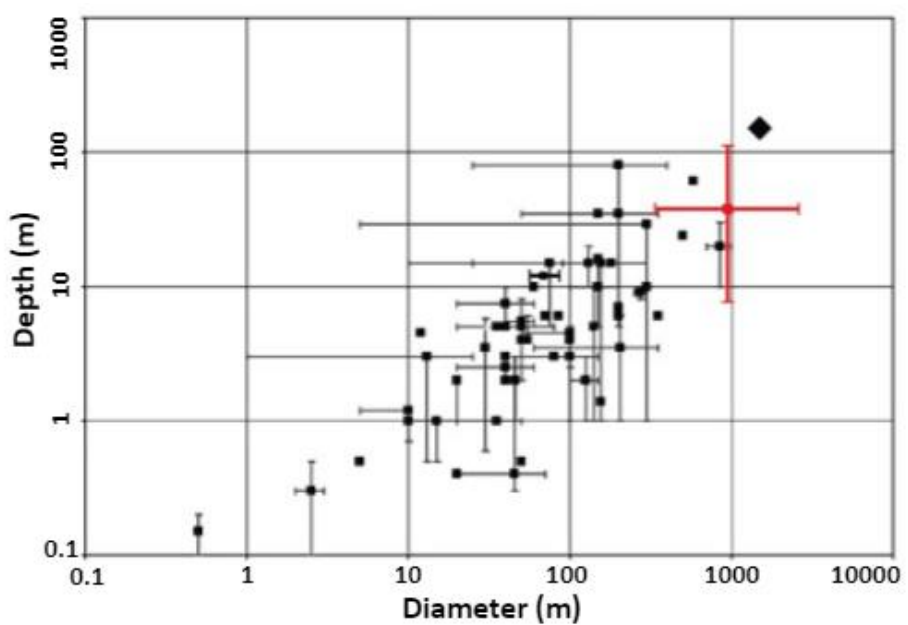
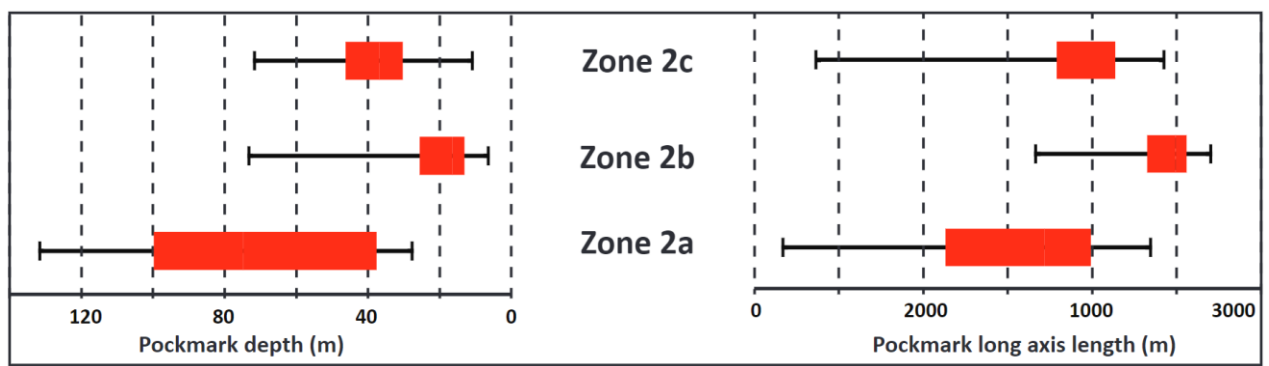


Figure 13

# South Atlantic Ocean

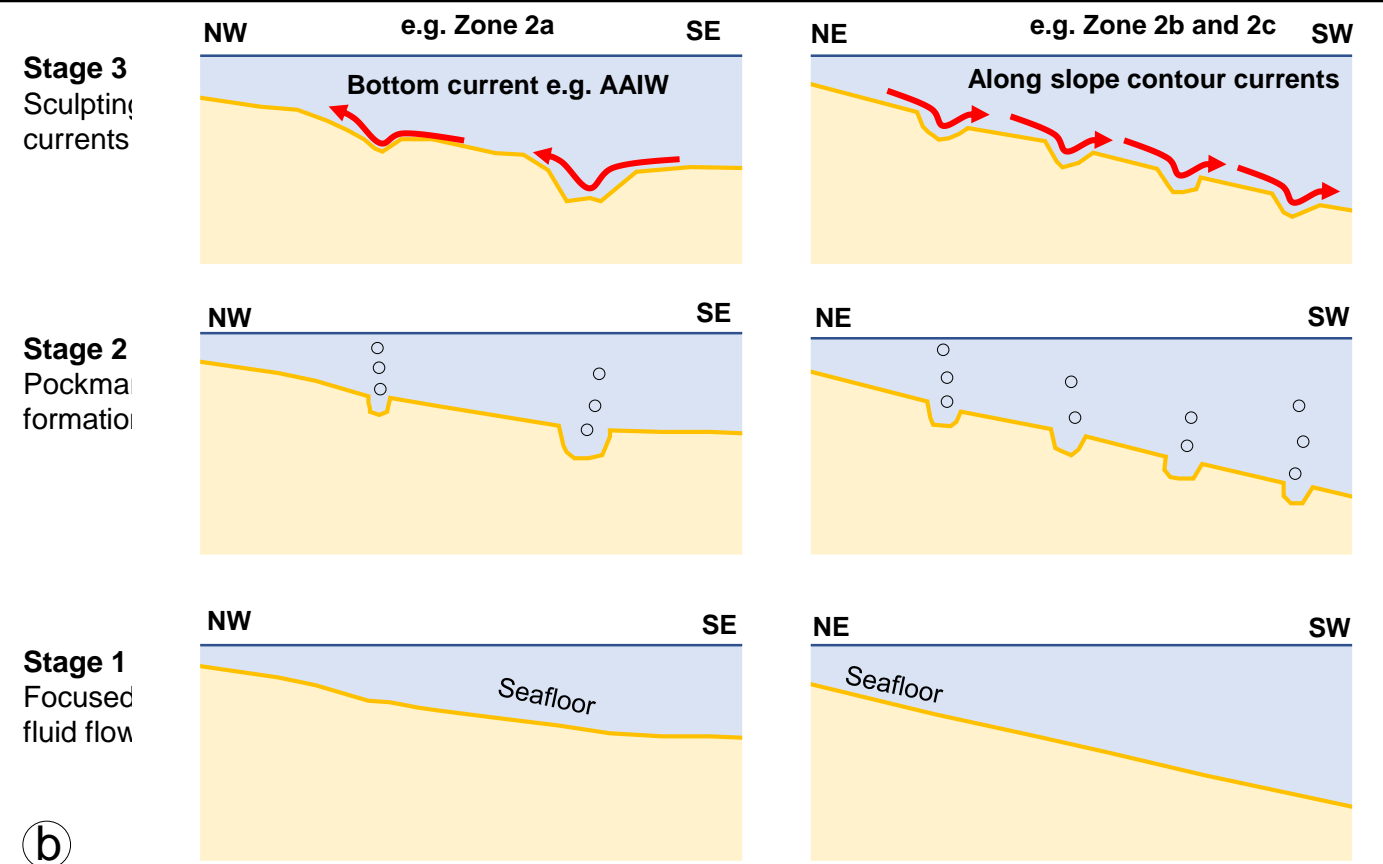
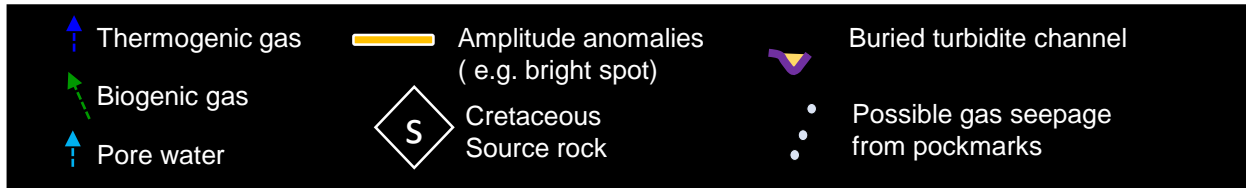
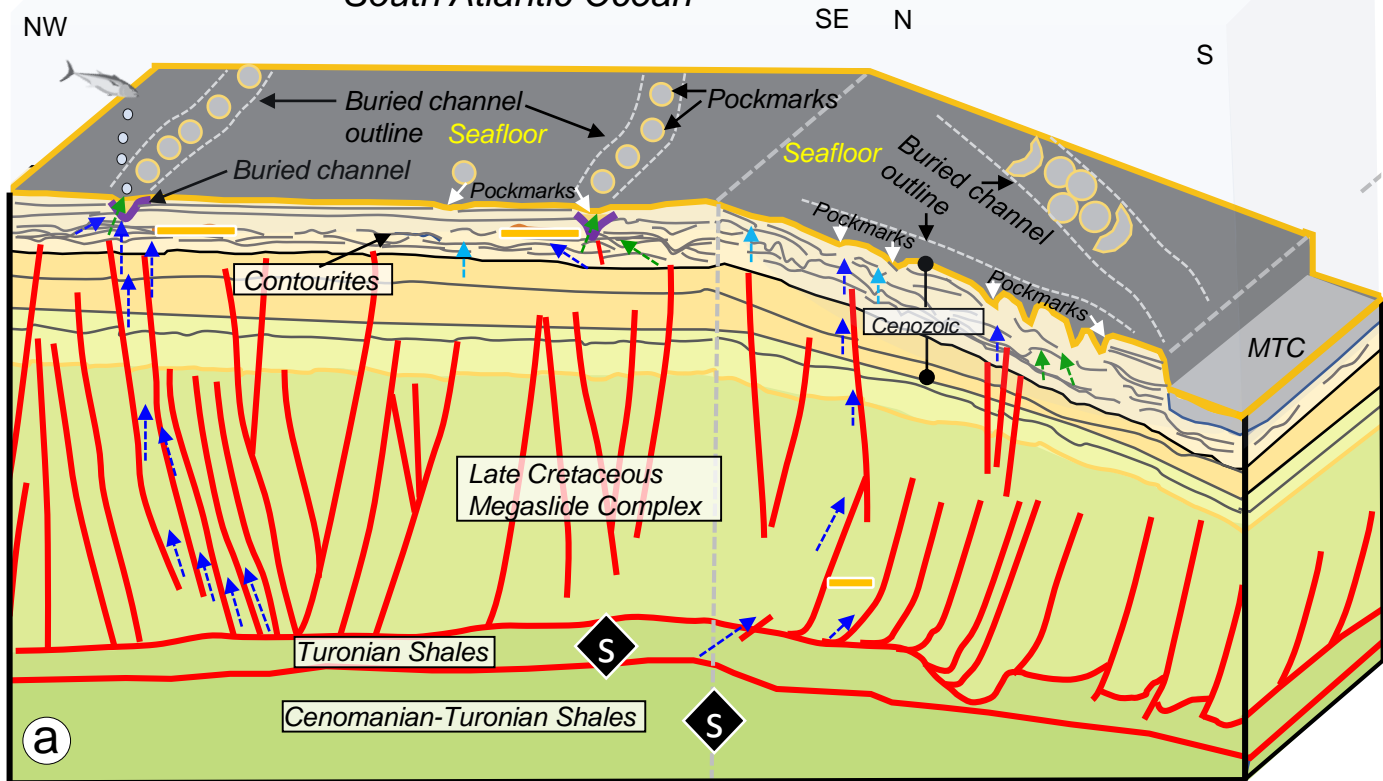


Figure 14

Table 1. Summary of the pockmark characteristics of each zone.

Zones	Pockmark types	No. Of individual pockmark	Average area (km)	Area range (km)	Average perimeter (km)	Perimeter range (km)	Average depth (m)	Depth range (m)	Diameter (long axis) (m)	Diameter range (m)	Water depth range (m)
2a	Circular	10	1.05	0.16 – 2.52	3.42	1.48 – 5.70	68.18	28.08 – 131.30	1396	663 - 2771	1100 - 1500
	Crescentic	2	3.82	2.38 – 5.25	7.51	6.22 – 8.80	121.81	114.60 – 129.03	2591	2360 - 2822	
2b	Circular	30	0.36	0.07 – 1.34	2.04	0.96 – 4.12	21.77	7.23 – 72.86	607	306 - 1326	872 - 1500
2c	Circular	4	0.59	0.24 – 0.85	2.79	1.82 – 3.37	44.41	23.52 – 72.86	890	617 - 1061	More than 1500 m
	Elongated	2	2.14	1.57 – 2.71	5.59	4.76 – 6.42	51.99	32.62 – 71.34	2219	1813 - 2625	
	Comet	2	0.64	0.47 - 0.82	2.89	2.49 – 3.30	47.05	45.54 – 48.57	979	947 - 1011	